

TOPICAL REVIEW • **OPEN ACCESS**

Hydrogen from wastewater by photocatalytic and photoelectrochemical treatment

To cite this article: Adriana Rioja-Cabanillas *et al* 2021 *J. Phys. Energy* **3** 012006

View the [article online](#) for updates and enhancements.



TOPICAL REVIEW

OPEN ACCESS

RECEIVED
4 August 2020REVISED
14 October 2020ACCEPTED FOR PUBLICATION
27 November 2020PUBLISHED
18 December 2020

Original content from this work may be used under the terms of the [Creative Commons Attribution 4.0 licence](#).

Any further distribution of this work must maintain attribution to the author(s) and the title of the work, journal citation and DOI.



Hydrogen from wastewater by photocatalytic and photoelectrochemical treatment

Adriana Rioja-Cabanillas¹ , David Valdesueiro² , Pilar Fernández-Ibáñez¹ and John Anthony Byrne^{1,*}

¹ Nanotechnology and Integrated BioEngineering Centre, School of Engineering, University of Ulster, Newtownabbey, BT37 0QB, United Kingdom

² Delft IMP B.V., Molengraaffsingel 10, Delft, 2629JD, The Netherlands

* Author to whom any correspondence should be addressed.

E-mail: j.byrne@ulster.ac.uk

Keywords: hydrogen production, wastewater, photocatalysis, photoelectrochemical cell

Abstract

In recent years, the intensification of human activities has led to an increase in waste production and energy demand. The treatment of pollutants contained in wastewater coupled to energy recovery is an attractive solution to simultaneously reduce environmental pollution and provide alternative energy sources. Hydrogen represents a clean energy carrier for the transition to a decarbonized society. Hydrogen can be generated by photosynthetic water splitting where oxygen and hydrogen are produced, and the process is driven by the light energy absorbed by the photocatalyst. Alternatively, hydrogen may be generated from hydrogenated pollutants in water through photocatalysis, and the overall reaction is thermodynamically more favourable than water splitting for hydrogen. This review is focused on recent developments in research surrounding photocatalytic and photoelectrochemical hydrogen production from pollutants that may be found in wastewater. The fundamentals of photocatalysis and photoelectrochemical cells are discussed, along with materials, and efficiency determination. Then the review focuses on hydrogen production linked to the oxidation of compounds found in wastewater. Some research has investigated hydrogen production from wastewater mixtures such as olive mill wastewater, juice production wastewater and waste activated sludge. This is an exciting area for research in photocatalysis and semiconductor photoelectrochemistry with real potential for scale up in niche applications.

1. Introduction

The current society is based on a linear production route, where the extraction of raw matter follows its industrial conversion into products, and its disposal as waste. This linear practice creates long-term problems because resources are limited and inefficiently used. The impact of this approach includes climate crisis, water pollution and reduction of biodiversity. Therefore, it is necessary to adopt different strategies conforming to the circular economy concept, where products and materials are in the economy as long as possible.

Wastewater has a great potential for resource recovery, being a source of nutrients such as phosphorus and nitrogen, materials including precious metals, and also a potential source for energy recovery. Conventional wastewater treatment plants are energy intensive, however, energy can be extracted from wastewater in diverse forms, including electricity, heat or fuels, as methane or hydrogen. Biogas production by anaerobic digestion is one of the most utilized methods for energy recovery from wastewater [1]. In this process, bacteria degrade the organic waste in the absence of oxygen to produce biogas, a gas mixture mostly composed of methane and carbon dioxide. Anaerobic digestion has been and is widely used in wastewater treatment plants around the world.

Hydrogen production is another promising approach to energy recovery from wastewater. Hydrogen is considered a clean energy carrier for the transition to a decarbonized society fuelled by renewable energy.

Its use in combustion or fuel cells generates only water resulting in zero carbon emissions and the high gravimetric heating value makes hydrogen a competitive energy carrier. In 2019, the International Renewable Energy Agency reported that more than 95% of hydrogen production came from fossil fuel based processes, such as steam-methane reforming and oil and coal gasification [2]. This fact highlights the urgent need to develop alternative and sustainable H₂ production processes, which may include recovery from wastewater.

Hydrogen can be generated from wastewater using biological processes. Wastewater has a high organic content making it a good candidate for hydrogen production via fermentation. Possible biohydrogen production methods include photo-fermentation and dark fermentation [3]. In photo-fermentation, photosynthetic bacteria powered by sunlight transform organic compounds into hydrogen and CO₂. Dark fermentation is a complex process in which several groups of bacteria participate in a series of biochemical reactions to convert organic substrates into biohydrogen. Often, dark fermentation is coupled to photo-fermentation; the organic acids, by-products of dark fermentation, are then converted to hydrogen by the photosynthetic bacteria during photo-fermentation [4]. An alternative bio-based technology to recover energy from wastewater is the use of microbial fuel cells (MFC). MFC use bacteria on the anode to oxidize the organic matter and inject electrons, where these electrons can be used to produce electricity or hydrogen at the cathode. MFC are considered a promising technology for wastewater treatment and energy recovery; however the slow electron transfer, low power generation, membrane fouling and low rate of microbes growth impede the rapid scaling-up of MFC [5, 6].

Among non-biological processes, an interesting approach is the use of photocatalysis to produce hydrogen from wastewater. Photoexcitation of the photocatalyst results in charge carrier formation with the necessary electrochemical reduction potentials to drive hydrogen evolution. In 1972, Fujishima and Honda reported for the first time photoelectrolytic water splitting to produce hydrogen and oxygen using a UV excited single crystalline TiO₂ electrode [7]. Since then, research in the photocatalysis field gained attention producing a substantial number of studies. While extensive research has been carried out in either photocatalytic hydrogen production or degradation of organic compounds, only a limited number of studies focus on hydrogen production from the degradation of components in wastewater. This review is focused on photocatalysis and photoelectrochemistry for the simultaneous recovery of energy and the removal of pollutants from wastewater.

The present article starts with an overview of the fundamentals, materials and the parameters used to evaluate the performance of photocatalytic processes (section 2) and photoelectrochemical cells (PECs) (section 3). The following section reviews hydrogen production from several wastewater compounds, which are categorized in groups, using both photocatalysis and photoelectrochemistry (section 4). This section focuses in discussing materials used, possible mechanisms and performance of these processes. Finally, this review concludes with a critical evaluation of the current limitations on this field and future opportunities.

2. Photocatalysis

2.1. Fundamentals

In photocatalysis, a semiconductor is irradiated with photons with energy equal to or greater than the band gap energy, resulting in the excitation of electrons from the valence band (VB) to the conduction band (CB). The photo-excited electron leaves a positively charged hole in the VB. These charge carriers are referred to as an electron-hole pairs. The charge carriers can recombine in the semiconductor bulk dissipating energy as heat or light or they can migrate to the surface of the semiconductor. At the surface, they can undergo charge transfer processes driving redox reactions with chemical species which are adsorbed at the surface of the photocatalyst.

Photocatalysis has been widely studied for the degradation of organic pollutants and extensive information can be found in previous reviews [8–11]. The organic pollutants can either undergo direct oxidation by holes, indirect oxidation by reactive oxygen species including hydroxyl radicals, or they may be transformed by a reductive route involving CB electrons. The most common electron acceptor in photocatalytic oxidation reactions is molecular oxygen since it is abundant in the air and is reasonably soluble in aqueous solutions. The oxygen is reduced by the CB electrons to form the superoxide radical anion (O₂^{•-}). Subsequent reduction reactions lead to H₂O₂, •OH, and eventually H₂O. A representation of this process is shown in figure 1(a).

Photocatalysis has also been investigated for hydrogen production through water splitting, as detailed described in several reviews [12–15]. The photogenerated holes are used to oxidize water molecules to evolve oxygen, while the photo-generated electrons in the CB reduce protons and evolve hydrogen, as shown in figure 1(b). However, photocatalytic hydrogen production from water splitting is a challenging reaction because it is thermodynamically unfavourable ($\Delta G^\circ = + 237 \text{ kJ mol}^{-1}$) requiring a high energy input and the transfer of four electrons. It should be recognized that technically, uphill thermodynamic processes are

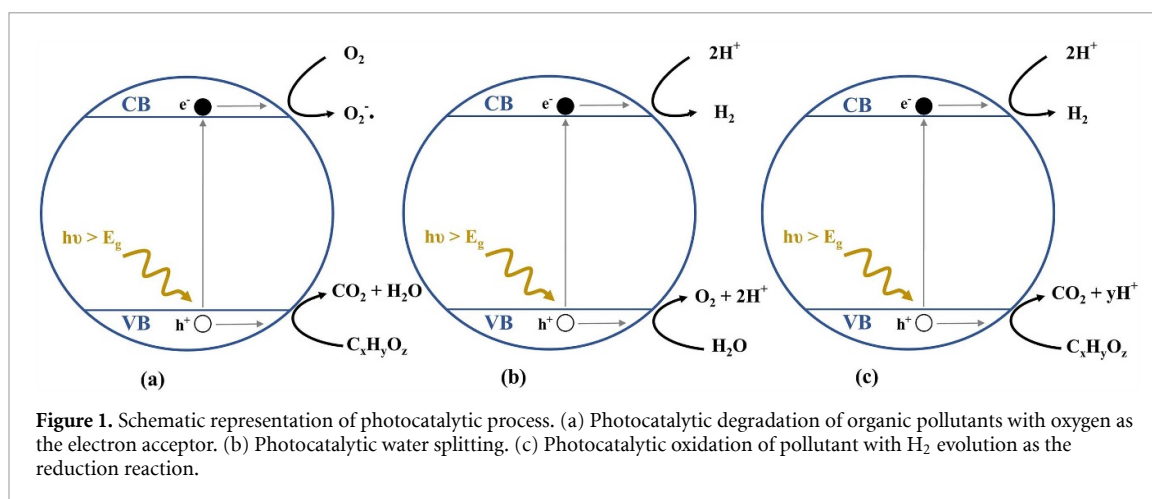


Figure 1. Schematic representation of photocatalytic process. (a) Photocatalytic degradation of organic pollutants with oxygen as the electron acceptor. (b) Photocatalytic water splitting. (c) Photocatalytic oxidation of pollutant with H_2 evolution as the reduction reaction.

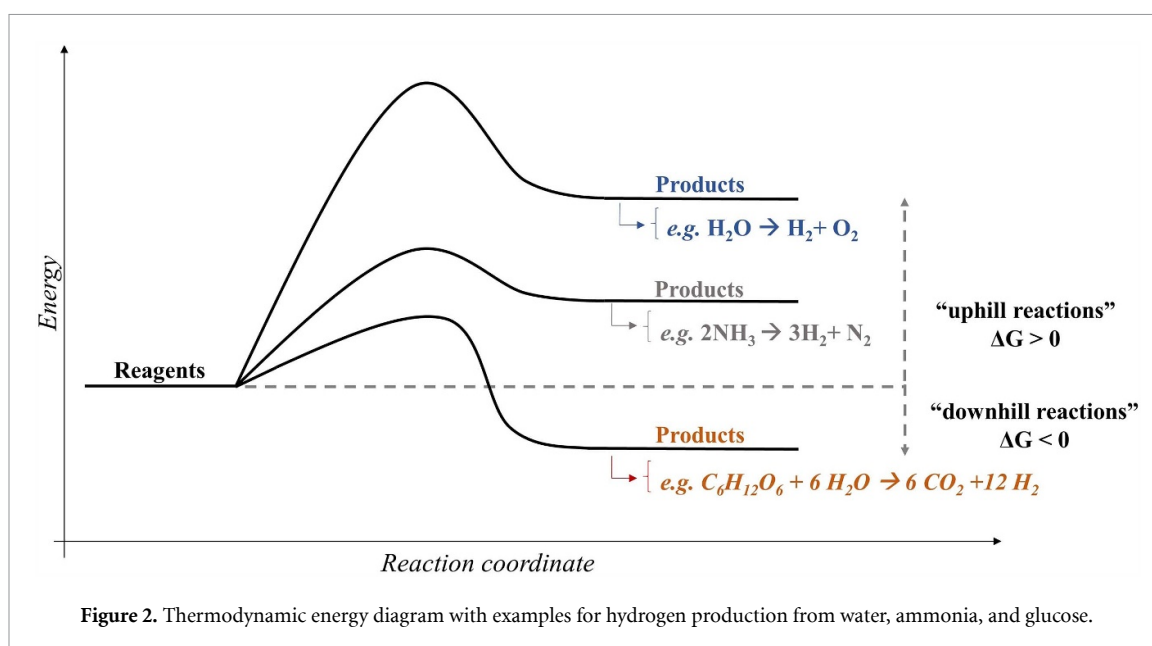
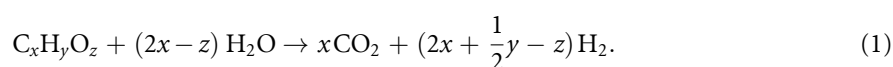


Figure 2. Thermodynamic energy diagram with examples for hydrogen production from water, ammonia, and glucose.

photosynthetic, however, to avoid confusion, in this review both uphill and downhill reactions will be referred as photocatalytic. Hydrogen production from the oxidation of other compounds with reactions requiring less energy or being thermodynamically favourable ($\Delta G^\circ < 0$) have also been investigated. This is schematically represented in figure 2. These compounds can donate electrons and scavenge the VB holes while also acting as a source of protons. There are many compounds present in wastewater that could act as a hydrogen source.

Most studied compounds have been organic, but this is also possible with inorganic compounds as, e.g. ammonia. In this application, the photo-generated holes are used to oxidize the unwanted compounds, which can take place through direct oxidation or indirect oxidation via hydroxyl radicals ($\bullet OH$). The photo-generated electrons reduce the protons to form hydrogen. A schematic representation of this process is shown in figure 1(c), with the oxidation of a generic organic compound. The photocatalytic oxidation of organic substances to form hydrogen is also referred as photoreforming and it follows the general equation given in (1).



The ability of a semiconductor to perform the desired redox reactions depends on the band gap energy and the band edge potentials for the VB and the CB. For the reactions to be thermodynamically possible, the CB edge potential should be more negative than the desired reaction reduction potential and the VB edge potential should be more positive than the desired reaction oxidation potential. In the water splitting reaction, the CB should be more negative than the hydrogen evolution reaction (HER) potential (0 V vs NHE at pH 0), and the VB should be more positive than the oxygen evolution potential (+1.23 V vs NHE at pH 0).

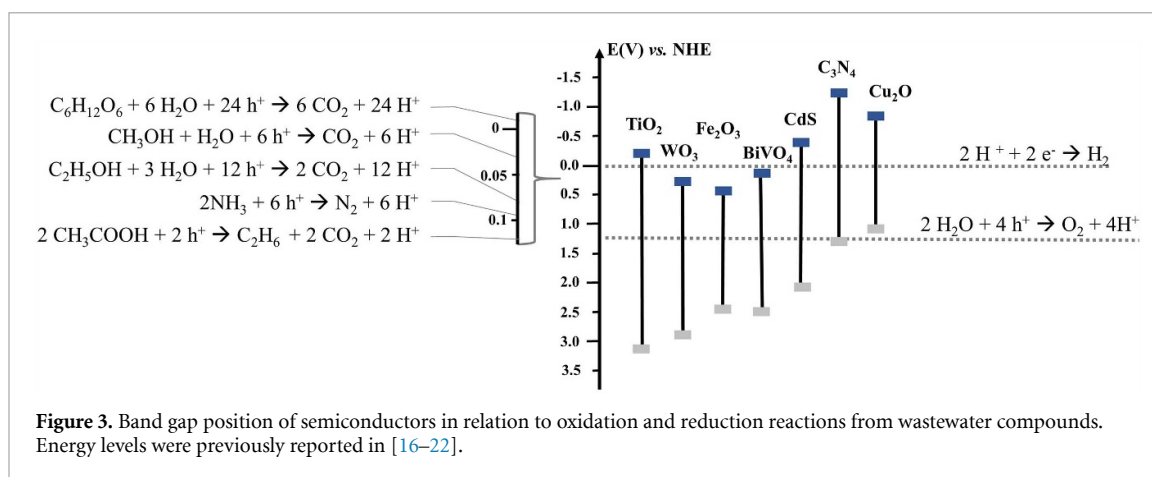


Figure 3. Band gap position of semiconductors in relation to oxidation and reduction reactions from wastewater compounds. Energy levels were previously reported in [16–22].

For the oxidation of wastewater pollutants, the CB needs to be more positive than the oxidation potential of the pollutants. These potentials are more negative than the potential for water oxidation, requiring less energy for the overall reaction. The CB and VB of several semiconductor materials, together with the oxidation and reduction potential of these reactions are given in figure 3.

The ideal semiconductor material for photocatalytic hydrogen production from wastewater compounds would have the following general requirements: suitable band edges position, good light absorption, efficient charge transport, chemical and photochemical stability, low overpotentials for the desired reduction and oxidation reactions, low cost and abundant. It is important to consider that almost half of the incident solar energy on the earth's surface is in the visible region ($400 \text{ nm} < \lambda < 800 \text{ nm}$), and therefore, for solar applications the photocatalyst should be able to utilize both the UV and visible photons.

2.2. Materials

While a wide range of materials have been investigated for photocatalytic hydrogen production [12–15], the present review will focus on the materials reported for H₂ production coupled to the oxidation of pollutants found in wastewater. Titanium dioxide is the most reported photocatalyst to investigate the coupling of H₂ production to the degradation of compounds found in wastewater [23–30]. Other materials as cadmium sulphide (CdS) [31, 32] and graphitic carbon nitride [33, 34] have also been reported for H₂ production from wastewater compounds.

Titanium dioxide (TiO₂) is employed in a wide variety of fields, ranging from energy applications such as hydrogen production and CO₂ reduction, to environmental applications as water treatment, air purification and water disinfection [35]. TiO₂ exists as three different polymorphs: anatase, rutile and brookite.

Its properties include high photo-activity, low cost, low toxicity and good chemical and thermal stability. Nevertheless, it suffers from fast electron–hole recombination and a large band gap. TiO₂ band gap is 3.2 eV for anatase, 3.0 eV for rutile, and ~ 3.2 eV for brookite [35]. This wide band gap limits the light absorption to the ultraviolet range, which just accounts for 4%–5% of the solar spectrum, consequently, limiting its practical application.

Developments to achieve visible light absorption by TiO₂ include doping, metal deposition, dye sensitization and coupled semiconductors [16]. Non-metal doping has been extensively researched, being nitrogen one of the most promising non-metal dopants that has achieved visible light absorption [36]. Nitrogen is easily inserted in the TiO₂ structure since it has a high stability, small ionization and its atomic size is similar to oxygen [37]. Other promising non-metal dopants are carbon and sulphur [38, 39]. Alternatively, the generation of oxygen rich TiO₂ has been reported to produce an increase in the Ti–O–Ti bond strength and an upward shift in the VB, achieving visible light absorption [40]. Doping with metals as chromium, cobalt, vanadium and iron has also been reported to improve the light absorption [16]. Dye sensitization has been considered as one of the most effective strategies to extend the spectral response into the visible region, benefiting from the knowledge of dye sensitized solar cells. Moreover, coupling TiO₂ with other semiconductors has also resulted in an improvement of the light absorption and a reduction of the recombination losses [41].

A commercially available TiO₂ product, Degussa (Evonik) P25, has been often used as a benchmark in research. It contains a combination of the polymorphs anatase and rutile with proportions of around 80% anatase and 20% rutile. This configuration enhances the photoactivity since the rutile phase, which has a

more positive CB potential, can act as electron sink for the photogenerated electrons of the anatase phase [16].

When TiO₂ is used for HER, usually metal co-catalysts are added. Since the work function of noble metals is typically larger than TiO₂, the photogenerated electrons transfer from the semiconductor CB to the metal [35]. Pt has been one of the most used co-catalysts for HER since it has the largest work function among the noble metals, creating a stronger electron trapping ability and has a low activation energy for proton reduction [16, 35]. Pt co-catalyst ability strongly depends in its particle size and loading [35].

CdS is a widely researched visible light photocatalyst. It has been investigated in diverse applications, such as hydrogen production, carbon dioxide reduction to hydrocarbons or pollutants degradation [20]. CdS is characterized by a narrow bandgap of 2.4 eV, which enables the absorption of light until 516 nm [20]. It exhibits good photochemical properties and quantum efficiency [42, 43]. However, it suffers from photo-corrosion, since the photogenerated holes react with the sulphur ions oxidizing them to sulphur [44]. CdS low stability makes difficult its application in industry. Some of the strategies to improve CdS stability and inhibit photo-oxidation include the addition of surface protective layers, constructing heterojunctions and combining them with microporous and mesoporous materials [31, 45].

Graphitic carbon nitride (g-C₃N₄) has received lot of attention as visible light photocatalyst, and it has been reported to be a promising photocatalyst for a diverse number of applications including H₂ production [46]. g-C₃N₄ is usually produced by thermal condensation of nitrogen-rich precursors. Its polymeric nature allows the modification of properties such as morphology, conductivity and electronic structure which modifies the bandgap energy and bandgap edges potential position [21]. g-C₃N₄ photocatalytic activity and efficiency have been improved using several strategies. Heteroatom doping and copolymerization have been employed to modify the electronic band structure to enhance light absorption [47]. Moreover, the heterojunction with other semiconductors as CdS [48] or TiO₂ [49] have been reported to achieve an improved separation of the photogenerated charges [21].

2.3. Efficiency

The photocatalytic performance can be evaluated using quantum efficiency. The quantum efficiency or yield is defined as the useful photo-conversion events per absorbed photons at a determined wavelength. The useful events are usually calculated by the reaction rate. This is given in (2) where r is the reaction rate given in number of molecules converted per second, and Φ_{pa} is the flux of absorbed photons expressed as number of photons per second. However, it is challenging to determine the absorbed photons in the semiconductor. Therefore, the external or apparent quantum efficiency, which is also referred as photonic yield, is usually used instead [50]. It can be defined as the useful events per incident photons in the system at a determined wavelength. This expression is given in (3), where r is the reaction rate given in number of molecules converted per second and Φ_{pi} is the flux of incident photons expressed as number of photons per second. The incident photons can be measured using radiometric or actinometric procedures. Moreover, the external quantum efficiency takes into account the efficiency of the overall process including the efficiency of the material absorbing photons as well as catalyzing the reaction and the efficiency of the reactor design [50].

$$QE(\lambda) = \frac{r}{\Phi_{pa}} \quad (2)$$

$$EQE(\lambda) = \frac{r}{\Phi_{pi}} \quad (3)$$

If one is using a polychromatic radiation source then the formal quantum efficiency (FQE) should be reported, normally integrating the number of photons which can be utilized by the semiconductor in question. Of course, for many semiconductors the true solar efficiency will be very low due to only a small proportion of the solar spectrum being utilized.

Additionally, the performance of a photocatalytic hydrogen production process can also be evaluated using the solar-to-hydrogen (STH) conversion efficiency (η_{STH}), which relates chemical hydrogen energy produced to the solar energy. This expression is shown in (4), where Φ_{H_2} is the hydrogen rate in mol s⁻¹ m⁻², $G_{H_2}^\circ$ the Gibbs free energy of hydrogen formation and P is the photon flux in mW cm⁻² measured for a light source with a spectra equal to air mass global (AM) 1.5 [51].

$$\eta_{STH} = \left[\frac{\Phi_{H_2} \cdot G_{H_2}^\circ}{P} \right]_{AM\ 1.5G} \quad (4)$$

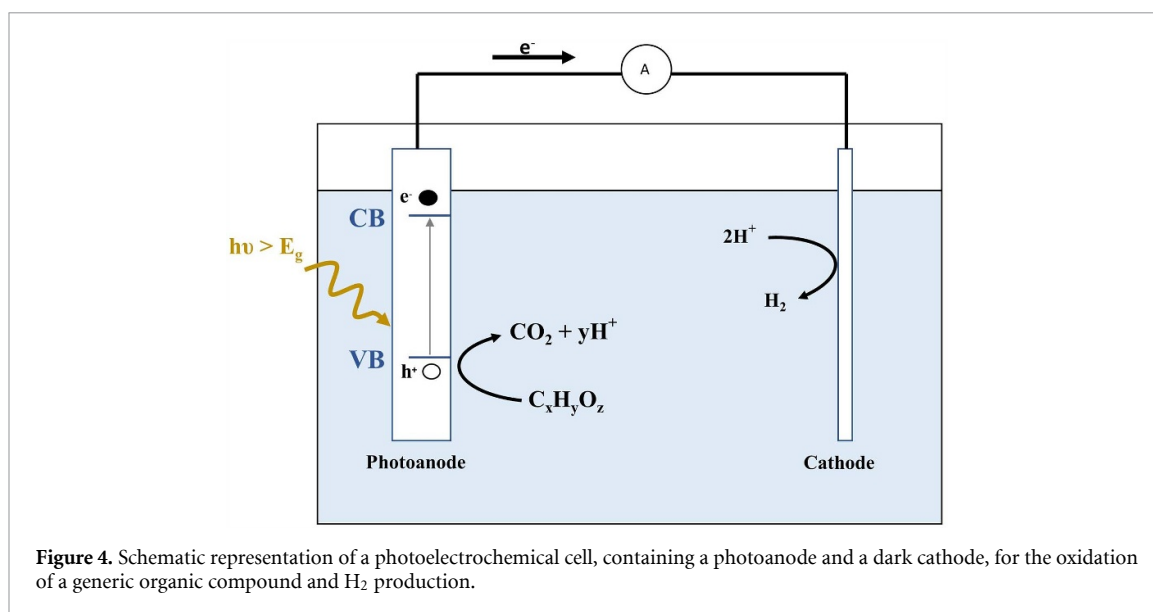


Figure 4. Schematic representation of a photoelectrochemical cell, containing a photoanode and a dark cathode, for the oxidation of a generic organic compound and H₂ production.

3. Photoelectrochemical cells

3.1. Fundamentals

An approach to enhance the efficiency of photocatalysis is the use of electrochemically assisted photocatalysts in a PEC. In this configuration, the oxidation and reduction reactions are performed by two different electrode materials that are connected through an external circuit. The oxidation is driven by the holes in the (photo)anode, while the electrons travel from the photoanode through the external circuit to the (photo)cathode, where the reduction reaction takes place. This process is schematically represented in figure 4. When a PEC is utilized to produce a fuel (e.g. hydrogen) from solar energy it can be referred as photosynthetic cell. Similarly, when the PEC is employed to produce electricity from the photodegradation of substances, it can be defined as photo fuel cell [52]. In systems where wastewater compounds are being oxidized in a PEC to generate H₂, depending on the thermodynamics of reaction, the system can also produce electricity and therefore being a combination of both cells; not clearly defined as one or the other. Moreover, a system without applied bias, where hydrogen is produced by a flow of current, could also be considered a photo fuel cell.

PECs can be used with different configurations, i.e. semiconductor photoanode with metallic cathode, semiconductor photocathode with metallic anode, or photoanode with photocathode. These cells are driven by the potential difference between the Fermi levels of the two electrodes. For a typical n-type semiconductor photoanode, the Fermi level is close to the CB while for a typical p-type semiconductor photocathode the Fermi level is close to the VB [53]. If the PEC uses a dark anode or cathode, these potentials are ideally dependent on the oxidation and reduction reaction potentials, respectively. If the reaction oxidation and reduction potentials have the right positions with respect to the CB and VB, the cell produces electric power in open circuit voltage. When this is not the case, an external voltage can be applied to drive the reactions.

With electrochemically assisted photocatalysis, an external electrical bias can be applied to assist the reactions. This may allow the use of semiconductor photoanodes with more positive CB potentials than the H⁺/H₂ reaction and which would not drive HER purely photocatalytically.

3.2. Materials

Titanium dioxide is the most used photoanode material for H₂ production from wastewater compounds [54–57]. Other photoanode materials that have also been used for H₂ production are tungsten trioxide, bismuth vanadate and hematite [58–60]. Concerning the cathode material, platinum is widely used [54, 55, 61, 62], while cuprous oxide is a common choice for photocathode [57].

3.2.1. Photoanodes

Titanium dioxide (TiO₂), is as well the most used semiconductor material for photoanodes. Its properties and applications have been described in the previous section. When compared with other photoanodes semiconductor materials as tungsten trioxide, bismuth vanadate or hematite, titanium dioxide shows good charge transport properties and a very high hole diffusion length, which is in the order of 10⁴ nm [58]. However, TiO₂ has one of the lowest theoretical STH conversion efficiency just accounting for around 2.2%,

due to its excitation being limited to the UV region [59]. One of the strategies studied to improve activity and reduce recombination losses, is to synthesize one- or two-dimensional nanostructures which increases the specific surface area and decreases internal resistance. A very popular approach is the nano-engineering of TiO_2 to form either dispersed or aligned self-organized nanotubes (TNT) [63]. Other used strategies include non-metal doping, co-catalyst deposition, dye sensitization and coupled semiconductors as explained previously [16].

Tungsten trioxide (WO_3), is a very popular metal oxide semiconductor used for photoanodes. It has been extensively researched for water splitting applications. It has a bandgap of 2.5–2.8 eV, absorbing light in the visible range up to 500 nm which accounts for 12% of the solar radiation on earth surface [60]. Its theoretical STH conversion efficiency is around 4.8% [58], and it has a modest hole diffusion length of around 150 nm [58]. Moreover, its CB is positioned at positive potentials of around +0.4 V vs NHE [17], therefore a bias is necessary to drive the HER. Unfortunately, its stability is limited to acidic environment [58]. Some strategies to improve the activity of WO_3 include the enhancement of light absorption with anion doping as C [64] or N [65] or forming heterojunctions with other semiconductors as $\text{WO}_3/\text{BiVO}_4$ [66].

Bismuth vanadate (BiVO_4) is the most popular visible light absorption semiconductor used as a photoanode and has attracted interest for water-splitting applications. BiVO_4 occurs in three polymorphs, from which monoclinic scheelite is the one being used as photoanode. It has a bandgap of 2.4 eV, a high theoretical STH conversion efficiency of 9.1% [59] and its CB potential is located slightly under that the HER potential [67]. However, it suffers from fast electron–hole recombination and a low charge mobility, and consequently an external bias is always necessary to obtain significant photocurrents [59]. In order to increase BiVO_4 carrier concentration doping with elements as Mo or W has been studied [68, 69]. Other strategies to improve BiVO_4 activity include the loading of co-catalysts as Co–Pi [70] to decrease the bias potential and help the oxidation reaction or the heterojunction with other semiconductors as SnO_3 or WO_3 to have a more efficient electron–hole separation [71, 72].

Hematite ($\alpha\text{-Fe}_2\text{O}_3$), is considered a very promising metal oxide photoanode since it has a narrow bandgap of around 2 eV, allowing to absorb light beyond 600 nm [59]. Therefore, its maximum theoretical STH conversion efficiency is around 15% [19]. Moreover, $\alpha\text{-Fe}_2\text{O}_3$ presents a good chemical stability and it is inexpensive and abundant. Its CB is situated at positive potentials of around 0.4 V vs NHE [19], therefore, it is necessary to apply a bias to drive hydrogen production. Nevertheless, it has a very low hole diffusion length of around 2–4 nm and a low electron mobility which limits its performance [60]. Strategies to improve $\alpha\text{-Fe}_2\text{O}_3$ conductivity and activity include, doping with elements as W, Mo and Nb [73–75], loading of co-catalysts as Co–Pi or $\text{Ni}(\text{OH})_2$ [55, 76] or surface passivation with Al_2O_3 [77].

3.2.2. Photocathodes

The choice of p-type materials for photocathodes is limited due to their low stability in contact with aqueous electrolyte [78]. Some strategies to improve the performance of the photocathode include the use of protective layers that improve stability and the deposition of co-catalysts to enhance the reduction ability [79–81].

Cuprous oxide (Cu_2O), is a popular photocathode choice, it has a band gap of 2 eV and a theoretical STH conversion efficiency of 18% [80]. Its CB is well positioned for water reduction, around 0.7 V vs NHE more negative than hydrogen evolution potential [22]. However, the potentials for reduction from Cu_2O to Cu and oxidation to CuO are within the band gap, reducing its stability [82]. There are several research studies that report improved stability by adding protective layers as ZnO [79]. Moreover, co-catalysts as Pt had been added to enhance the reduction activity [80].

Copper based chalcogenide semiconductors have also been proposed as promising photocathodes for hydrogen production [83]. One of them is $\text{CuIn}_x\text{Ga}_{1-x}\text{Se}_2$ (CIGS) which has a tuneable composition, with a band gap ranging from 1 eV to 1.7 eV and a large absorption coefficient [81]. Their activity have been enhanced adding protective layers and co-catalysts such as Pt [84]. However, CIGS include In and Ga which are scarce and expensive elements. Another type of chalcogenide photocathode is $\text{Cu}_2\text{ZnSnS}_4$ (CZTS), which has earth abundant elemental constituents, high absorption coefficient and small band gap, however; it suffers from low long-term stability [85]. The research to improve its activity has also focused into surface modification, adding protecting layers as TiO_2 and co-catalysts as Pt [81].

3.2.3. Dark cathode electrocatalysts

The selection of a cathode for HER benefits from an extensive research in the electrochemistry field. HER involves the adsorption of a proton on the electrocatalyst surface and the desorption of hydrogen. For this reason, following Sabatier principle, the optimal catalytic activity will be achieved with a catalyst that achieves intermediate binding energy between the substrate and the catalyst [86]. The catalyst activity is as well dependent on the pH of the electrolyte, and in general, HER activities in alkaline electrolyte are lower

than in acid. Consequently, the majority of the research is done in acid environment. For HER, the catalyst closer to the optimum intermediate binding energy is Pt. Platinum has generally the best performance as hydrogen production catalyst, it has a low overpotential and high reaction rates in acidic environment [61]. Pt foil and wires, together with Pt supported carbon are the most common cathodes used in the studies for H₂ production from driven photoelectrochemical oxidation of substances in wastewater.

Other catalysts with a good performance are Ru, Rh, Ir and Pd. However, all these noble metal catalysts, together with Pt, have a high cost and they are scarce, which makes challenging their large-scale application. Different approaches have been widely researched to find electrocatalysts with low cost and good performance. Two strategies that have been used to improve activity and reduce the cost of using noble metal catalysts are nanostructuring the catalyst to achieve a large surface to volume ratio, and forming alloys which reduce the catalyst loading [87, 88].

Non-noble metal alloys have also been used for HER, Ni-based electrodes are preferred cathodes for hydrogen production in basic environment as Ni–Mo [88]. Transition metals chalcogenides as carbides and phosphides have also showed HER activity. Chalcogenides as MoS₂ showed activity for HER due to their sulphided Mo-edges with and overpotential close to Pt [89]. Similarly, WS₂ also demonstrates HER activity [90] as well as their selenides forms MoSe₂ and WSe₂ [91]. Tungsten carbides such as WC and W₂C, exhibit promising potential as HER catalysts [92]. Phosphides as CoP and Ni₂P are among the most HER active non-noble electrocatalysts [93, 94]. Alternatively, non-metals electrocatalysts options have also been explored as heteroatom doped graphene nanosheets [94] or carbon nitride [95].

3.3. Efficiency

When evaluating the performance of PECs, the external quantum efficiency is also referred as incident photon to current efficiency (IPCE), and the number of successful events can be evaluated by the photo-electrical current generated. This expression is given in (5), where λ is the wavelength of irradiation in nm, J is the photocurrent density given in mA cm⁻², P is the photon flux in mW cm⁻² at a particular λ , h is Plank's constant and c is the speed of light in vacuum [53].

$$\text{EQE}(\lambda) = \text{IPCE}(\lambda) = \frac{\Phi_e}{\Phi_{\text{pi}}} = \frac{J \cdot hc}{\lambda \cdot P_\lambda}. \quad (5)$$

Moreover, when evaluating the performance of PECs, η_{STH} can also be determined from the photocurrent density generated. This expression is shown in (6) where J is the photocurrent density given in mA cm⁻², V is the required potential in V derived from Gibbs free energy, η_f is the HER faradaic efficiency and P is the light power in mW cm⁻² measured with a light source with a spectra equal to AM global 1.5 [51]. It is important to note that J needs to be measured between the working and counter electrode in a two electrode PEC configuration. No bias potential should be applied in the evaluation of η_{STH} . Whenever a bias potential is applied between working and counter electrode to drive the reaction, the applied bias photon to current conversion efficiency (ABPE) can be derived, as shown in (7) [51]. In this expression V_{bias} is the applied voltage in V, which is subtracted from the required potential derived from Gibbs energy.

$$\eta_{\text{STH}} = \left[\frac{J \cdot V \cdot \eta_f}{P} \right]_{\text{AM 1.5G}} \quad (6)$$

$$\text{ABPE} = \left[\frac{J \cdot (V - V_{\text{bias}}) \cdot \eta_f}{P} \right]_{\text{AM 1.5G}} \quad (7)$$

For wastewater treatment applications, an UV source is commonly used as oppose to solar irradiation; therefore the power coming from the sun should be replaced by the power of the UV source.

4. H₂ production from wastewater

Wastewater includes every water stream that has been polluted by human utilization, therefore, its chemical composition varies greatly depending on its origin. Domestic wastewater, which derives from urban areas, is generally rich in microorganisms, organic materials, metals, and nutrients as phosphorous or nitrogen [96]. These effluents are usually treated at municipal wastewater treatment plants. On the contrary, industrial effluents are diverse, being originated by very different processes. Some industrial wastewaters have a similar chemical composition than domestic wastewater and can be treated in urban wastewater treatment plants, while other industrial effluents contain substances that need a specific and complex treatment process, as persistent organics, antibiotics or metals [97]. Finally, agricultural activities generate wastewater with a high

content of nitrogen compounds, due to excessive use of fertilizers and intensive farming [98], although agricultural wastewater normally cannot be collected and treated.

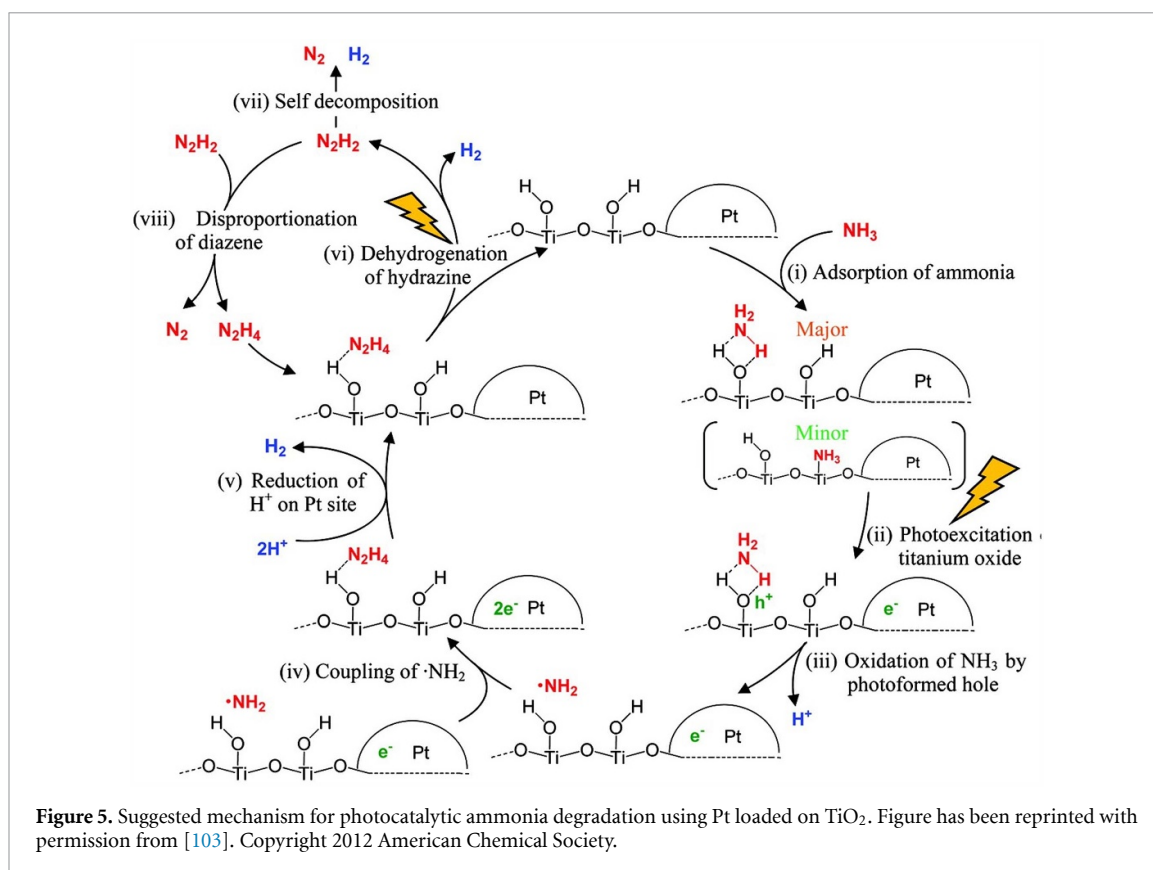
These wastewaters, originated by human activities, need to be treated to avoid pollution and protect the ecosystems. Therefore, coupling the production of hydrogen with the removal of pollutants represents a promising option to recover energy from wastewater and at the same time managing the water pollution issue. This section describes the studies that produced hydrogen coupled to the degradation of wastewater compounds, including the materials used and the possible mechanisms. The reviewed wastewater substances include nitrogen compounds, saccharides, phenolic compounds, alcohols, organic acids, aldehydes, and complex mixtures from oil mill wastewater, juice production wastewater and sludge from wastewater treatment plants.

4.1. Nitrogen compounds

Ammonia and urea, along with nitrates and nitrites, contribute to nitrogen pollution. Nitrogen pollution of water has deleterious effects including eutrophication and toxicity to the organisms living in the water body. The hazardous concentration of nitrogen in wastewater originate from diverse sources, as intensive farming and excessive fertilizer use [98]. Additionally, high nitrogen concentrations can also be found in either domestic and municipal sewage sludge and in wastewater from some industries [99].

In water, un-ionized ammonia (NH_3) exists in pH dependent equilibrium with ionized ammonium (NH_4^+), having a pKa of 9.25, when the pH is lower than the pKa, NH_4^+ is the major form and when the pH is higher than the pKa is NH_3 the major form. Therefore, one of the research focuses has been to determine which of the forms would have a higher photocatalytic oxidation rate. Several studies have revealed that ammonia in neutral form presents better oxidation rates compared to ionized ammonium [23, 100, 101]. Nemoto *et al* investigated the pH effect in the photocatalytic ammonia oxidation, testing a pH range from 0.68 to 13.7 [23]. The study reports that the evolution of gaseous products (N_2 and H_2) increased between the pH 9 and 10 and peaked at pH around 11, due to higher oxidation rates with neutral ammonia. Zhu *et al* reported how the oxidation rates obtained were proportional to the initial concentration of NH_3 and not the total content of NH_3 and NH_4^+ [100]. From this study, it was concluded that high oxidation rates are obtained when ammonia is in neutral form, even if better photocatalytic activity could be expected with positively ionized NH_4^+ and a negative photocatalyst surface charge, which occurs when the pH is higher than the photocatalyst point of zero charge and lower than the ammonium pKa. Wang *et al* compared the photocatalytic activity in acidic, basic and neutral environment using g- C_3N_4 as photocatalyst and reported higher rate of photocatalytic ammonia oxidation in basic solutions [101].

The most studied photocatalyst for ammonia oxidation has been TiO_2 [23, 102–104], covering how the co-catalyst material affects the activity and product selectivity [23, 102–104] and determining the possible reaction mechanism on H_2 production from ammonia decomposition [103]. Nemoto *et al* compared the activity of TiO_2 loaded with RuO_2 , Pt and both RuO_2 and Pt as co-catalysts for photocatalytic ammonia oxidation and hydrogen production [23]. The results showed that the N_2 gas produced was similar for all the co-catalysts; however, the H_2 production varied significantly. The photocatalyst loaded with Pt achieved the highest H_2 production and an external quantum yield of 5.1% at 340 nm, while the system with both co-catalysts produced a small amount of H_2 . The system loaded with RuO_2 did not produce any H_2 , showing that RuO_2 cannot reduce protons to form hydrogen. Altomare and Selli studied how the conversion and selectivity of ammonia oxidation to N_2 would be affected by the deposition of noble metals (Pt, Pd, Au and Ag) on the TiO_2 photocatalyst [102]. The experiments showed that all the metal-modified photocatalysts had better catalytic performance than the bare TiO_2 , with the exception of Au/ TiO_2 . The loaded photocatalyst that showed higher ammonia removal was Ag/ TiO_2 and the one that showed better selectivity towards N_2 was Pd/ TiO_2 . This latter study did not link the oxidation of ammonia to H_2 production. Yuzawa *et al* studied the mechanism of decomposition of ammonia to produce dinitrogen and hydrogen using TiO_2 photocatalyst loaded with Pt, Rh, Pd, Au, Ni and Cu [103]. Pt presented the best activity with high production rate of H_2 and N_2 and Cu the worse. The study concluded that the metal with larger work function would easily accept the photo-excited electrons to produce hydrogen. The mechanism proposed consisted in the predominant adsorption of ammonia to the Lewis acid site and some to the hydroxyl groups in TiO_2 . The TiO_2 is irradiated generating holes and electrons, where the holes migrate to the surface and the electrons to the Pt site. The photogenerated holes oxidize the adsorbed NH_3 to form amide radicals and protons, while the amide radicals can produce hydrazine. The hydrazine could produce diazene that would be decomposed to form N_2 and H_2 . The photogenerated electrons reduce the protons to form hydrogen in Pt [103]. This mechanism is represented in figure 5. Shiraishi *et al* investigated the photocatalytic hydrogen production from ammonia using TiO_2 loaded with Au and Pt [104]. Pt–Au/ TiO_2 showed a growth in hydrogen production rate compared to Pt/ TiO_2 , suggesting that alloying Au to Pt resulted in a decrease of the



Schottky barrier height at the interface between metal and TiO₂. The catalyst with the highest H₂ production rates consisted in a homogeneous mixture of 10% mol of Au and 90% mol of Pt loaded on TiO₂.

Photocatalytic ammonia oxidation has also been reported using metal free photocatalyst. Wang *et al* used an atomic single layer g-C₃N₄ as photocatalyst, achieving an ammonia removal of 80% of the initial concentration [101]. Both hydroxyl radicals and photogenerated holes were suggested to be responsible for the ammonia oxidation; in this study ammonia oxidation was not coupled to H₂ production.

The number of research papers reported on ammonia oxidation using PECs is much less than compared to photocatalysis [54, 105]. Wang *et al* used highly ordered TiO₂ nanotube arrays as a photoanode and Pt foil as cathode [105], reporting an ammonia removal of 99.9% under an applied bias of 1.0 V (not coupled to H₂ production). Kaneko *et al* used nanoporous TiO₂ film as photoanode, formed by P25 deposited on FTO glass and a Pt foil as a cathode [54]. The experiments showed a 150 A cm⁻² photocurrent and a production of 194 ml of H₂ and 63 ml of N₂ after 2 h with no bias applied under a pH of 14.1.

The reported studies of H₂ production driven by photocatalytic or photoelectrochemical oxidation of urea are scarce and their main focus is proving the feasibility of the process [24, 55, 106]. They include the study of surface modification and co-catalyst loading. Moreover, a comparison of the H₂ production rate from oxidation of urea, ammonia and formamide has also been studied [56].

Kim *et al* investigated the effect of dual surface photocatalyst modification in the production of hydrogen and oxidation of urea [24]. TiO₂ modified with both a noble metal, Pt, and an anion adsorbate [24]. The results showed that F-TiO₂/Pt achieved higher H₂ production rates than Pt/TiO₂, besides, F-TiO₂ did not show any H₂ production, highlighting the combined effect of surface anions and metal deposits to reduce charge recombination and improve electron transfer. Moreover, the effect of other anions as Cl⁻, ClO⁻ and Br⁻ was studied, resulting in only F⁻ to have an enhancement effect, Cl⁻ and ClO⁻ had no effect and Br⁻ inhibited the hydrogen production. These results were explained by the surface complexation among acidic Ti(IV) sites and basic anions, which is dependent on the hardness of the anions, being only F⁻ the one that has higher hardness than OH⁻. Furthermore, experiments with deuterated urea were performed, showing that H₂ production comes mainly from water molecules while urea acts as an electron donor.

Wang *et al* studied the feasibility of hydrogen production driven by urea or urine oxidation in a PEC [55]. In this work, the suitability of two photoanodes was studied, TiO₂ nanowires and α-Fe₂O₃ nanowires, both loaded with Ni(OH)₂ as urea oxidation co-catalyst. Pt was used as counter electrode. The viability of solar driven urea oxidation with Ni/TiO₂ as photoanode was reported using an unbiased cell, producing a current density of 0.35 mA cm⁻². Moreover, the feasibility of using directly urine was also studied, resulting in

comparable results to urea, highlighting the possibility of driving the production of hydrogen with the oxidation of urine. The effect of loading α -Fe₂O₃ with Ni(OH)₂ was studied, showing a negative shift in the onset potential of 400 mV, suggesting that Ni(OH)₂ is an efficient catalyst for urea oxidation. However, the use of α -Fe₂O₃ as photoanode required an external bias due to the low position of its CB. Xu *et al* investigated as well the role of Ni(OH)₂ as a co-catalyst in the photoelectrochemical oxidation of urea, not coupled to the production of hydrogen [106], by using a photoanode formed of Ti-doped, α -Fe₂O₃ and loaded with Ni(OH)₂. The addition of Ni(OH)₂ reduced the onset potential by 100 mV and increased the photocurrent density by four times, showing the enhanced effect of the use of Ni(OH)₂ as urea oxidation co-catalyst.

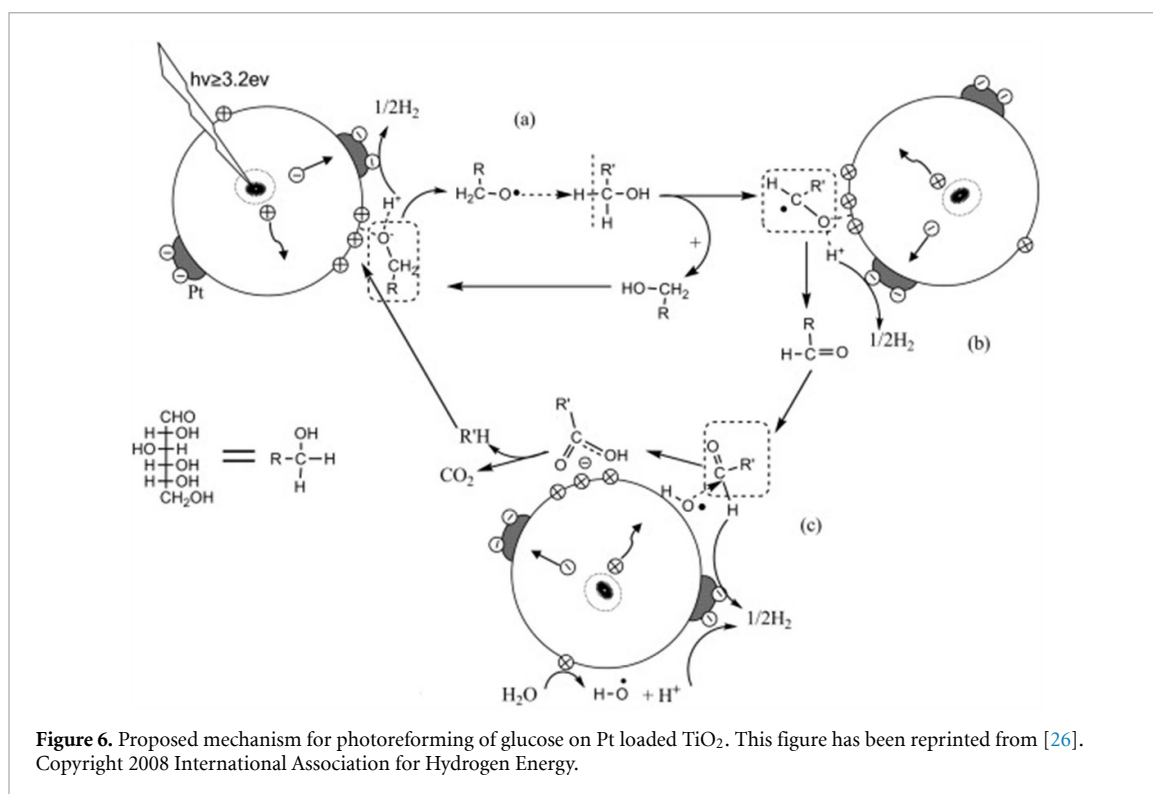
Pop *et al* focused their study in the comparison of the hydrogen production rates driven by oxidation of three nitrogen compounds found in wastewater: ammonia, urea and formamide [56]. The cell configuration combined a nanoparticulate TiO₂ photoanode and a mixture of carbon paste dispersing platinum nanoparticles (NPs) as cathode in the same electrode. This configuration was unbiased and used under UV illumination. The detected hydrogen production after 4 h was about 30, 140 and 240 mol in presence of ammonia, formamide and urea, respectively. From these results, urea proved to be the best choice for photoelectrochemical hydrogen production. Additionally, a cell configuration with a separated photoanode and cathode, applying 0.5 V bias was also tested. The results from the two configurations were compared after 50 min, in which the biased configuration reported a H₂ production rate of 2.7 mol min⁻¹ while the unbiased configuration reported a rate of 1.4 mol min⁻¹, highlighting the improved charge separation induced by the use of a bias.

4.2. Saccharides

Different saccharides compounds can be found wastewater; among them, cellulose is commonly found in domestic wastewater and effluents from industries as the paper industry [107].

Kawai and Sakata demonstrated the feasibility of producing hydrogen from Saccharides (C₆H₁₂O₆)_n, as saccharose ($n = 2$), starch ($n \approx 100$) and cellulose ($n \approx 1000$ – 5000), using a photocatalyst formed by RuO₂/TiO₂/Pt. A quantum yield of 1% at 380 nm was reported for cellulose in 6 M NaOH [108]. Moreover, Kondarides *et al* studied the hydrogen production from the photocatalytic reforming of several compounds including cellulose using a Pt/TiO₂ photocatalyst, proving the potential of cellulose for H₂ production [25]. Speltini *et al* investigated the photocatalytic hydrogen production from cellulose using a Pt/TiO₂ photocatalyst [109]. The study showed higher H₂ production rates with neutral pH and reported a H₂ production of 54 μ mol under UV-A irradiation. A degradation mechanism was also reported suggesting that cellulose depolymerizes and converts into glucose and other water-soluble products. Caravaca *et al* researched the photocatalytic H₂ production from cellulose using different metals as co-catalysts loaded in TiO₂. The highest H₂ production was reported with Pd and the lowest with Ni and Au, following the trend Pd > Pt > Ni \sim Au [110]. Even the H₂ production using Ni as co-catalyst was lower compared to the noble metals Pd and Pt; it was in the same magnitude, highlighting the possibility of using a no noble metal as co-catalyst. Moreover, the study suggested the possibility of the hydrolysis of cellulose taking place during irradiation to produce glucose, which could follow different pathways to produce hydrogen.

The photoreforming of glucose, which is proposed to be an intermediate in the cellulose photoreforming process, has been reported in several studies [25, 26, 111–113]. Kondarides *et al* studied the hydrogen production from the photocatalytic reforming glucose using a Pt/TiO₂ photocatalyst, reporting an external quantum efficiency of 63% at 365 nm [25]. Fu *et al* studied the effect of different parameters as pH and co-catalyst material and proposed a mechanism for the hydrogen production from photocatalytic reforming of glucose using a metal loaded photocatalyst [26]. The study reported the effect of different co-catalysts loaded in TiO₂, showing all of them a better activity than the bare TiO₂; the best activity was obtained using Pd and Pt and the worse with Ru and Ag, following the trend Pd > Pt > Au \approx Rh > Ag \approx Ru. Moreover, the variation of pH over a wide range resulted in an increasing H₂ production rate with increasing pH, with a plateau region from pH 5–9 and maximum peak at pH 11. The pK_a of glucose is around 12.3; therefore, higher rates of glucose oxidation are produced with glucose in its molecular form. In the proposed mechanism, the glucose is adsorbed preferentially in the uncoordinated Ti atoms through its hydroxyl group; it dissociates and then it is oxidized by a photogenerated hole. The radicals generated attack other glucose molecules, forming R-CHOH, which are deprotonated and further oxidized to [R-COOH]⁻ by the radical •OH. Lastly, [R-COOH]⁻ species are photo-oxidized by a hole to generate CO₂ via a photo-Kolbe reaction [26]. This mechanism is presented in figure 6. Chong *et al* investigated the glucose photoreforming mechanism using Rh/TiO₂ photocatalyst, reporting the production of arabinose, erythrose, glyceraldehyde, gluconic acid and formic acid (together with CO and CO₂ gas) [111]. In the suggested mechanism, glucose is oxidized into arabinose, then further oxidized into erythrose and ultimately into glyceraldehyde. These oxidation reactions take place through •OH radicals, which leads to the generation of formic acid and



hydrogen. Subsequently, formic acid is converted into CO or CO₂. Imizcoz and Puga studied photocatalytic hydrogen production from glucose using TiO₂ loaded with different metals as Au, Ag, Pt and Cu [112]. The study reported a catalyst efficiency following the trend Pt > Au > Cu > Ag, without significant differences between Cu and Au, proposing Cu as an inexpensive co-catalyst for hydrogen production. Bahadori *et al* researched the hydrogen production from glucose photoreforming using CuO or NiO loaded TiO₂ as photocatalyst [113]. The highest hydrogen production yield reported was 9.7 mol g_{cat}⁻¹ h⁻¹ using 1 wt% CuO on P25.

Other semiconductor materials as WO₃ and α-Fe₂O₃ have also been studied using a PEC for hydrogen production from photoreforming of glucose. Esposito *et al* reported how a thin film WO₃ photoanode presented a good photocatalytic activity for H₂ production from glucose photoreforming using a tandem cell device [114]. Wang *et al* investigated the possibility of using Ni(OH)₂ as co-catalyst for glucose oxidation (not coupled to H₂ production) in a PEC, reporting an increased activity for Ni(OH)₂ loaded in α-Fe₂O₃ [62].

4.3. Phenolic compounds

Phenolic compounds are found in significant quantities in wastewater from effluents of several industries as oil refining, petrochemicals, resin manufacturing and pulp, but also in agricultural and domestic wastewaters [97, 115]. Phenolic compounds are considered toxic and its discharge without treatment produces harmful effects in the aquatic systems [116]. The photocatalytic degradation of phenolic compounds has been widely studied [117]. However, only few cases coupled the photocatalytic oxidation of phenolic compound to H₂ production [24, 27, 33, 57, 118–120], demonstrating the feasibility of this process.

Hashimoto *et al* investigated the photocatalytic H₂ production in presence of different aliphatic and aromatic compounds with suspended Pt/TiO₂ [27], demonstrating the production of hydrogen in presence of phenol. Moreover, the study showed an increased rate of H₂ production in presence of phenol in alkaline conditions over acidic conditions. Languer *et al* reported that the photocatalytic phenol degradation over TiO₂ nanotubes produced hydrogen at a rate of about 0.06 μmol h⁻¹ cm⁻² [119]. Kim *et al* demonstrated the feasibility of hydrogen production coupled to photocatalytic degradation of 4-chlorophenol [24]. The study involved the activity comparison of the following photocatalysts: TiO₂/Pt, F-TiO₂/Pt and P-TiO₂/Pt. The highest H₂ production rate was obtained with F-TiO₂/Pt and the lowest with TiO₂/Pt. However, the good activity of F-TiO₂/Pt was limited to acidic region since the fluorides desorb at the alkaline region. P-TiO₂/Pt had higher H₂ production range than TiO₂ for all the pH range. Lv *et al* used S doped two-dimensional g-C₃N₄ for the photocatalytic hydrogen production from phenol, achieving a H₂ production rate of 127.4 μmol h⁻¹ and an external quantum efficiency of 8.35% at 400 nm [33].

In PECs, several photoanode materials have been tested. Wu *et al* studied the effect of the photoanode and photocathode materials on the voltage and current generated in the phenol degradation and hydrogen production [57]. Different photoanode and photocathode nanostructures, as nanorods (NRs), NPs and nanowires (NWAs) were tested from TiO₂, CdS, CdSe and Cu₂O. It was demonstrated that the open circuit voltage depends not only on the Fermi level between the photoelectrodes, but also on crystal facet for the same semiconductor materials with different microstructures. The best phenol removal efficiency was achieved with the combination of the photoanode TiO₂ NRs/FTO and the photocathode C/Cu₂O NWAs/Cu. This combination reached a phenol removal rate of 84.2% and an overall hydrogen production rate of 86.8 mol cm⁻² in 8 h. Park *et al* demonstrated the feasibility of hydrogen production driven by the photoelectrochemical degradation of phenol using improved multi-layered BiO–TiO₂/Ti electrodes [118]. The electrodes were formed by an under layer of TaO–IrO, a middle layer of BiO_x–SnO₂, and an upper layer of BiO–TiO₂ which covered both sides of Ti foil. The study showed that bismuth doping, even at high concentration, increased TiO₂ conductivity, while preserving the original photoelectrochemical properties. Li *et al* studied the photoelectrocatalytic hydrogen production in presence of phenol using Bi/BiVO₄ as photoanode [120]. The study reported a hydrogen production rate of 27.8 mol cm⁻² h⁻¹.

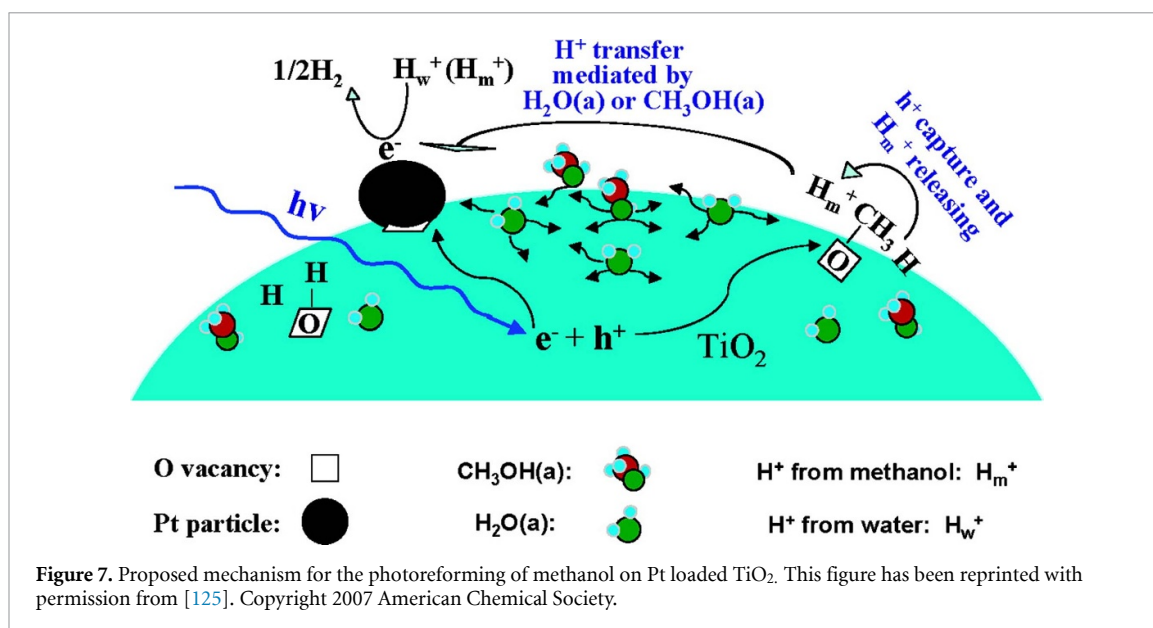
4.4. Alcohols

Although alcohols are not expected to be abundant and common substances in municipal wastewater, they may be present in some industrial wastewater [121]. The production of H₂ from photocatalytic oxidation of alcohols has been extensively studied, mainly methanol, ethanol, and glycerol oxidation.

Kawai and Sakata demonstrated the feasibility of producing hydrogen by photoreforming of methanol [122]. The study reports the highest H₂ production rate Pt and an apparent quantum yield of 44% at 380 nm with a photocatalyst formed by RuO₂/TiO₂/Pt. In the proposed reaction mechanism, methanol forms an intermediate, formaldehyde, which further oxidizes to formic acid and finally decomposes to CO₂ and H₂. Chiarello *et al* studied the effect of loading different noble metal co-catalysts to a TiO₂ photocatalyst in the photoreforming of methanol [123]. Among the investigated co-catalysts (Ag, Au and Pt), Pt showed the highest hydrogen production rate. Moreover, Naldoni *et al* studied the difference between loading TiO₂ photocatalyst with Au or Pt, concluding that photogenerated electrons are more easily transferred to the Pt NPs to reduce protons, than to Au [124]. Chen *et al* studied the mechanism of the photocatalytic reaction of methanol for hydrogen production on Pt/TiO₂ [125]. The proposed mechanism (figure 7) involves the formation of H₂ on Pt sites, in which the proton transfer to the Pt sites is mediated by the adsorbed water and methanol molecules. Most of the protons that form H₂ in the Pt sites come from water and not from methanol. The study demonstrates that the surface species of CH₂O, CH₂OO and HCOO were formed. Moreover, an increase in Pt loading generated a decrease on methanol adsorption, which suggest that Pt atoms occupy sites for methanol adsorption [125]. Ismael studied the use of a Ru doped TiO₂ photocatalyst for the hydrogen production from methanol, reporting an enhancement on the activity due to the decrease in the band gap and a larger surface area [126]. The highest activity was reported doping with of 0.1% mol of Ru. In another study, Chen *et al* reported the possibility of using a low cost photocatalyst formed by carbon coated Cu/TiO₂ (C/Cu/TiO₂) for hydrogen production from methanol [127]. This photocatalyst produced a H₂ yield of 269.1 mol h⁻¹ which is comparable to 290.8 mol h⁻¹, the yield produced with Pt/TiO₂.

Liu *et al* investigated the interaction between CuO_x–TiO₂ and its effect on the photocatalytic production of hydrogen from methanol [128]. The highest H₂ production was reported with CuO_x/TiO₂-0 0 1 which has the highest Cu₂O dispersion and strongest interaction. Jiménez-Rangel *et al* study the performance of g-C₃N₄/NiOOH/Ag as photocatalyst for the photoreforming of methanol, obtaining a maximum H₂ yield of 350.6 mol h⁻¹. The hydrogen yield of the combined g-C₃N₄/NiOOH/Ag photocatalyst resulted significantly higher compared to the yield of g-C₃N₄, g-C₃N₄/NiOOH or g-C₃N₄/Ag alone [34]. Hojamberdiev *et al* studied the use of a photocatalyst composed of g-C₃N₄ Ni(OH)₂ and halloysite nanotubes for the production of hydrogen from methanol [129]. This photocatalyst presented a higher H₂ production rate (18.42 mol h⁻¹) than g-C₃N₄/Ni(OH)₂ (9.12 mol h⁻¹) or g-C₃N₄ (0.43 mol h⁻¹). This enhancement was attributed to charge separation being the holes trapped by the halloysite nanotubes and the electrons transferred to Ni(OH)₂.

Ethanol has been extensively studied as a sacrificial agent for H₂ production [25, 31, 32, 130–136]. Sakata and Kawai studied the photocatalytic production of hydrogen from ethanol [130]. The study reports the production of hydrogen, methane, and acetaldehyde. Moreover, different co-catalyst loaded in TiO₂ were studied as Ni, Pd, Pt and Rh, being Pt the one with the highest H₂ production rate and with a reported external quantum yield of 38% at 380 nm. Kondarides *et al* studied the hydrogen production from the photocatalytic reforming of ethanol with a Pt/TiO₂ photocatalyst, reporting an external quantum efficiency of 50% at 365 nm [25]. Yang *et al* researched the photocatalytic production of hydrogen from ethanol using metal loaded TiO₂ as photocatalyst and compared it to the H₂ production from other alcohols [131]. Pt and



Pd presented higher H₂ production rates than Rh. Moreover, it was suggested that the hydrogen production over Pt/TiO₂ is governed by the solvation of the alcohol, following the H₂ production the following trend: methanol \approx ethanol > propanol \approx Isopropanol > *n*-butanol. Sola *et al* investigated the effect of the morphology and structure of Pt/TiO₂ photocatalysts on the hydrogen production from ethanol [132]. The study showed an improved performance for the Pt/TiO₂ photocatalysts with higher surface area and lower pore size. The best performing photocatalyst was found to be Pt/TiO₂ with an average pore size of 29.1 nm and a surface area of 51 m² g⁻¹, reporting an apparent quantum yield of 5.14%. Acetic acid, 2,3-butanediol and acetaldehyde were the main products in the liquid phase, finding a higher concentration of 2,3-butanediol with lower pore size. Puga *et al* studied the hydrogen production from photocatalytic ethanol oxidation over Au/TiO₂, obtaining as main products acetaldehyde in the liquid phase and H₂ in the gas phase with a volumetric proportion of 99%, while the other gaseous product detected were CH₄, C₂H₄, C₂H₆, CO and CO₂ [133].

Deas *et al* used Au loaded on TiO₂ nanoflowers as photocatalyst for hydrogen production from ethanol, reporting a hydrogen production rate of 24.3 mmol g⁻¹ h⁻¹, compared to only 12.1 mmol g⁻¹ h⁻¹ obtained with Au/P25 [134]. This enhancement was ascribed to the thin and crystalline anatase sheets of the nanoflower petals which reduce the bulk recombination. Pajares *et al* investigated the use of WC as TiO₂ co-catalyst for the photocatalytic hydrogen production from ethanol, reporting an enhancement of 40% on the H₂ yield compared to P25 [135]. Zhang *et al* investigated the effect of Ti³⁺ defects of Au/TiO₂ on the hydrogen production from ethanol [136]. The study reported an increased activity with higher defects, concluding that oxygen vacancies on TiO₂ rich in defects, facilitates the adsorption of ethanol and hole transfer. Ryu *et al* studied the photoreforming of ethanol using CdS attached on microporous and mesoporous silicas as photocatalyst. The study suggests that the photoactivity was dependent on the silica cavity size, which partially controls the CdS particle size [31]. Cebada *et al* studied the use of Ni/CdS as photocatalyst for the hydrogen production from ethanol, proving that higher Ni content resulted in increased hydrogen production [32].

Antoniadou *et al* studied the hydrogen production from ethanol using a PEC chemically biased [137]. The cell had two compartments, with a TiO₂ photoanode in an acidic electrolyte compartment and a Pt cathode in alkaline electrolyte compartment. The study reported an IPCE of 96% at 360 nm and proved that the photoreforming of ethanol is more efficient than photocatalytic water splitting. Adamopoulos *et al* investigated the effect of adding a top layer of TiO₂ to a WO₃ photoanode in the hydrogen production from ethanol using a biased PEC [138]. Carbon black loaded on carbon paper was used as cathode. Increased current density and hydrogen production were reported when using the TiO₂/WO₃ bilayer photoanode; this improvement was ascribed to the lower number of recombination sites.

H₂ production from photoreforming of glycerol has also been widely studied [25, 139–144]. Kondarides *et al* studied the hydrogen production from the photocatalytic reforming of glycerol, reporting an external quantum efficiency higher than 70% at 365 nm with a Pt/TiO₂ photocatalyst and 1 M of glycerol [25]. Fu *et al* studied the mechanism of photoreforming polyols as glycerol using a Pt/TiO₂ photocatalyst, proposing that just the H atoms connected to hydroxyl C atoms can form H₂ while the C atoms are oxidized to CO₂

[139]. For non-OH bonded C atoms, the bond H and C atoms form products in the form of alkanes as CH₄ or C₂H₆. Bowker *et al* investigated the photocatalytic reforming of glycerol using Pd and Au modified TiO₂ and proposed a possible mechanism [140]. Hydrogen production rate from Pd was four times larger than the one of Au. The mechanism suggests that H₂ is produced through the dissociation of adsorbed glycerol molecules with the associated production of CO, when using Pd/TiO₂. Subsequently, the CO reacts with oxygen radical at the metal surface to produce CO₂ freeing sites. Montini *et al* studied the hydrogen production from glycerol using Cu/TiO₂ photocatalyst [141]. Hydrogen and carbon dioxide were the main products in gas phase, and 1,3-dihydroxypropanone and hydroxyacetaldehyde in liquid phase. Moreover, Chen *et al* reported a quantum efficiency of 24.9% at 365 nm and hydrogen production rate of 17.6 mmol g⁻¹ h⁻¹ from glycerol using Cu/TiO₂ as photocatalyst [142]. Daskalaki and Kondarides studied the hydrogen production from photoreforming of glycerol over Pt/TiO₂, reporting H₂ and CO₂ as the only products in gas phase and methanol and acetic acid as intermediates in liquid phase [143]. Naffati *et al* reported a hydrogen production rate of 2091 mol g⁻¹ from glycerol using a photocatalyst consisting of TiO₂ loaded with Pt and carbon nanotubes (CNT) [144].

Hydrogen production from glycerol has been also demonstrated using PECs using a TiO₂ photoanode [145], or a TiO₂ photoanode functionalized with CdS [146].

4.5. Organic acids and aldehydes

Other compounds that can be part of the organic waste contained in wastewater are organic acids and aldehydes [147, 148]. Patsoura *et al* studied the hydrogen production and simultaneous degradation of formic acid, acetic acid and acetaldehyde over a Pt/TiO₂ photocatalyst [149]. The study reported a hydrogen production after 20 h of 183.2 mol from acetic acid and 72.5 mol from acetaldehyde.

et al researched the photocatalytic hydrogen production in presence of oxalic acid, formic acid and formaldehyde using a Pt/TiO₂ photocatalyst [28]. The study reported that the photocatalytic activity of these electron donors follows the trend of oxalic acid > formic acid > formaldehyde which agrees with the order of adsorption affinity of these electron donors on TiO₂.

Imizcoz and Puga investigated the photoreforming of acetic acid using Cu/TiO₂ as photocatalyst [150]. Hydrogen production from acetic acid was enhanced by including a photoreduction step to control the oxidation stage of Cu. On the contrary, when Cu was used directly, its passivation resulted in a high decarboxylation, producing mainly CH₄ instead of H₂.

4.6. Wastewater mixtures

The feasibility of photocatalytic H₂ production from wastewater mixtures such as olive mill wastewater (OMW), juice production wastewater and waste activated sludge has been demonstrated [29, 30, 112, 151].

OMW contains a high load of organics varying from 40 to 220 g l⁻¹ [152]. The main components found on this wastewater are oil, grease, polyphenols and sugars [151]. Badawy *et al* studied the photocatalytic degradation of OMW with simultaneous hydrogen production using nanostructured mesoporous TiO₂ as photocatalyst [29]. TiO₂ loading and pH were the main factors affecting the photocatalytic degradation and H₂ production in this study. The maximum hydrogen production was 38 mmol after 2 h at a pH of 3 and a photocatalyst concentration of 2 g l⁻¹. The organic pollutants contained in OMW enhanced the H₂ production, by scavenging holes and decreasing the electron hole recombination. Speltini *et al* investigated the effects of factors as photocatalyst concentration, pH and OMW concentration in H₂ production, using Pt/TiO₂ as photocatalyst and UV-A irradiation [151]. The study reports an apparent quantum yield of 5.5 × 10⁻³ at 366 nm and the production of 44 mol of H₂ after 4 h of UV-A irradiation, using a photocatalyst concentration of 2 g l⁻¹, OMW concentration of 3.35 v/v, and a pH of 3. Moreover, the H₂ yield produced by OMW was compared to glucose, which have been considered a good sacrificial donor for H₂ production, and similar production rates were obtained.

Imizcoz and Puga demonstrated the feasibility of photocatalytic hydrogen production using wastewater from a juice production industry, which contains high amounts of saccharides [112]. The study reported a H₂ yield of 115 mol g_{cat}⁻¹ h⁻¹ using Au/TiO₂ as photocatalyst.

The simultaneous H₂ production and degradation of waste activated sludge from wastewater treatment processes was investigated by Liu *et al*, using Ag/TiO₂ as photocatalyst, proving the possibility of this process [30].

All the materials used in the reviewed works for H₂ production by photocatalytic and photoelectrochemical oxidation of each wastewater component are summarize in tables 1 and 2.

Table 1. Summary of the materials used in the H₂ production from photocatalytic degradation of wastewater compounds.

Waste	Photocatalyst	Co-catalyst	Maximum efficiency (%)	Reference
Ammonia	TiO ₂	Pt or RuO ₂	EQE _(340nm) = 5.1	[23]
	TiO ₂	Pt, Rh, Pd, Au, Ni or Cu	—	[103]
	TiO ₂	Pt–Au	—	[104]
Urea	F-TiO ₂	Pt	—	[24]
Cellulose	RuO ₂ /TiO ₂	Pt	EQE _(380 nm) = 1	[108]
	TiO ₂	Pt	—	[25]
	TiO ₂	Pt	—	[109]
	TiO ₂	Pd, Pt, Ni or Au	—	[110]
Glucose	TiO ₂	Pt	EQE _(365 nm) = 63	[25]
	TiO ₂	Pd, Pt, Au, Rh, Ag or Ru	—	[26]
	TiO ₂	Rh	—	[111]
	TiO ₂	Pt, Au, Ag or Cu	—	[112]
	TiO ₂	CuO	—	[113]
Phenol	TiO ₂	Pt	—	[27]
	TiO ₂	—	—	[119]
	S-g-C ₃ N ₄	—	EQE(400 nm) = 8.35	[33]
4-chlorophenol	F-TiO ₂ or P-TiO ₂	Pt	—	[24]
Methanol	TiO ₂ /RuO ₂	Pt or Pd	EQE _(380 nm) = 44	[122]
	TiO ₂	Ag, Au or Pt	—	[123]
	TiO ₂	Au or Pt	FQE = 14	[124]
	Ru- TiO ₂	Pt	—	[126]
	TiO ₂	Pt	EQE _(355 nm) = 2.9	[125]
	TiO ₂ /C	Cu/C	—	[127]
	g-C ₃ N ₄	NiOOH/Ag	—	[34]
g-C ₃ N ₄	Ni(OH) ₂ /Al ₂ Si ₂ O ₅ (OH) ₄	—	[129]	
Ethanol	TiO ₂	Pt	EQE _(365 nm) = 50	[25]
	TiO ₂	Ni, Pd, Pt or Rh	EQE _(380 nm) = 38	[130]
	TiO ₂	Pt, Pd or Rh	FQE = 10	[131]
	TiO ₂	Pt	EQE = 5.14	[132]
	TiO ₂	Au	—	[130]
	TiO ₂	Au	—	[134]
	TiO ₂	Au	—	[136]
	TiO ₂	WC	—	[135]
	CdS	—	—	[31]
CdS	Ni	—	[32]	
Glycerol	TiO ₂	Pt	EQE _(365 nm) = 70	[25]
	TiO ₂	Pt	—	[139]
	TiO ₂	Pd or Au	—	[140]
	TiO ₂	Cu	—	[141]
	TiO ₂	Cu	EQE _(365nm) = 24.9	[142]
	TiO ₂	Pt	—	[143]
	TiO ₂	CNT-Pt	—	[144]
Formic acid	TiO ₂	Pt	—	[149]
	TiO ₂	Pt	—	[28]
Acetic acid	TiO ₂	Pt	—	[149]
	TiO ₂	Cu	—	[150]
Oxalic acid	TiO ₂	Pt	—	[28]
Acetaldehyde	TiO ₂	Pt	—	[149]
Formaldehyde	TiO ₂	Pt	—	[28]
OMW	TiO ₂	—	—	[29]
	TiO ₂	Pt	EQE _(366 nm) = 5.5 × 10 ⁻³	[151]
Juice industry wastewater	TiO ₂	Au	—	[112]
Sludge	TiO ₂	Ag	—	[30]

5. Conclusions

This review has described the potential of wastewater as source for energy recovery, using photocatalytic oxidation of pollutants coupled to hydrogen production. The production of hydrogen from pollutants and wastes is energetically more favourable than the production of hydrogen from water splitting.

Using suspensions of photocatalytic particles has been the most common approach to date, while only a limited number of works have adopted the use of PECs. PEC represent a promising option since this

Table 2. Summary of the materials used in the H₂ production from degradation of wastewater compounds using photoelectrochemical cells.

Waste	Photoanode	(Photo)Cathode	Maximum efficiency (%)	Reference
Ammonia	TiO ₂	Pt	—	[54]
	TiO ₂	Pt/C	—	[56]
Urea	Ni(OH) ₂ loaded on TiO ₂ or α -Fe ₂ O ₃	Pt	—	[55]
	TiO ₂	Pt/C	—	[56]
Formamide	TiO ₂	Pt/C	—	[56]
Glucose	WO ₃	WC	EQE _(600 nm) = 80	[114]
	Ni(OH) ₂ loaded on α -Fe ₂ O ₃	Pt	—	[62]
Phenol	TiO ₂ NRs, TiO ₂ NTs/Ti, CdS and CdSe	C/Cu ₂ O/Cu and Cu ₂ O	IPCE _(380 nm) = 68	[57]
	BiO _x -TiO ₂ /Ti	SS	—	[118]
	Bi/BiVO ₄	Pt	—	[120]
Ethanol	TiO ₂	Pt	IPCE _(360nm) = 96	[137]
	TiO ₂ /WO ₃	Carbon black	—	[138]
Glycerol	TiO ₂	Pt	—	[145]
	TiO ₂ /CdS	Pt	—	[146]

configuration reduces the recombination losses within the system. Up to now there has been limited research focused on the optimization of the design of photocatalytic reactors or PECs to improve the overall system efficiency. More research is needed on materials that have already shown promising results for water splitting and which might show improved efficiencies as compared to pure TiO₂ for hydrogen production from wastewater.

Only a few studies have investigated hydrogen production coupled to the treatment of real or simulated wastewater and more studies are needed to assess the real application. It is extremely challenging to compare the performance from the different published works. Hydrogen production rates, when given, are measured under very different operating conditions and the quantum efficiencies are sometimes not reported. Therefore, following a systematic procedure in reporting photocatalytic performance would be beneficial for the evaluation of the different compounds. Nevertheless, hydrogen production linked to the degradation of pollutants in wastewater is an exciting area for research and may have true potential for scale up at least in niche applications.

Acknowledgments


The authors would like to acknowledge the funding from the European Union's Horizon 2020 research and innovation programme under the Marie Skłodowska-Curie Actions grant agreement No. 812574.

ORCID iDs

Adriana Rioja-Cabanillas  <https://orcid.org/0000-0001-9632-1615>

David Valdesueiro  <https://orcid.org/0000-0002-4557-8581>

Pilar Fernández-Ibáñez  <https://orcid.org/0000-0001-6877-4684>

John Anthony Byrne  <https://orcid.org/0000-0001-9527-7659>

References

- [1] Guest J S et al 2009 A new planning and design paradigm to achieve sustainable resource recovery from wastewater *Environ. Sci. Technol.* **43** 6126–30
- [2] Gielen D, Taibi E and Miranda R 2019 *Hydrogen: A Renewable Energy Perspective*, International Renewable Energy Agency (Abu Dhabi: IRENA)
- [3] Lin C Y, Lay C H, Sen B, Chu C Y, Kumar G, Chen C C and Chang J S 2012 Fermentative hydrogen production from wastewaters: a review and prognosis *Int. J. Hydrog. Energy* **37** 15632–42
- [4] Azwar M Y, Hussain M A and Abdul-Wahab A K 2014 Development of biohydrogen production by photobiological, fermentation and electrochemical processes: a review *Renew. Sustain. Energy Rev.* **31** 158–73
- [5] ElMekawy A, Hegab H M, Dominguez-Benetton X and Pant D 2013 Internal resistance of microfluidic microbial fuel cell: challenges and potential opportunities *Bioresour. Technol.* **142** 672–82
- [6] Do M H, Ngo H H, Guo W S, Liu Y, Chang S W, Nguyen D D, Nghiem L D and Ni B J 2018 Challenges in the application of microbial fuel cells to wastewater treatment and energy production: a mini review *Sci. Total Environ.* **639** 910–20
- [7] Fujishima A and Honda K 1972 Electrochemical photolysis of water at a semiconductor electrode *Nature* **238** 37–38
- [8] Herrmann J-M, Guillard C and Pichat P 1993 Heterogeneous photocatalysis: an emerging technology for water treatment *Catal. Today* **17** 7–20
- [9] Bahnemann D 2004 Photocatalytic water treatment: solar energy applications *Sol. Energy* **77** 445–59

- [10] Gaya U I and Abdullah A H 2008 Heterogeneous photocatalytic degradation of organic contaminants over titanium dioxide: a review of fundamentals, progress and problems *J. Photochem. Photobiol. C* **9** 1–12
- [11] Malato S, Fernández-Ibáñez P, Maldonado M I, Blanco J and Gernjak W 2009 Decontamination and disinfection of water by solar photocatalysis: recent overview and trends *Catal. Today* **147** 1–59
- [12] Ni M, Leung M K H, Leung D Y C and Sumathy K 2007 A review and recent developments in photocatalytic water-splitting using TiO₂ for hydrogen production *Renew. Sustain. Energy Rev.* **11** 401–25
- [13] Moniz S J A, Shevlin S A, Martin D J, Guo Z-X and Tang J 2015 Visible-light driven heterojunction photocatalysts for water splitting—a critical review *Energy Environ. Sci.* **8** 731–59
- [14] Ismail A A and Bahnemann D W 2014 Photochemical splitting of water for hydrogen production by photocatalysis: a review *Sol. Energy Mater. Sol. Cells* **128** 85–101
- [15] Maeda K 2011 Photocatalytic water splitting using semiconductor particles: history and recent developments *J. Photochem. Photobiol. C* **12** 237–68
- [16] Pelaez M et al 2012 A review on the visible light active titanium dioxide photocatalysts for environmental applications *Appl. Catal. B* **125** 331–49
- [17] Bamwenda G R and Arakawa H 2001 The visible light induced photocatalytic activity of tungsten trioxide powders *Appl. Catal. A* **210** 181–91
- [18] Cooper J K, Gul S, Toma F M, Chen L, Glans P A, Guo J, Ager J W, Yano J and Sharp I D 2014 Electronic structure of monoclinic BiVO₄ *Chem. Mater.* **26** 5365–73
- [19] Tamirat A G, Rick J, Dubale A A, Su W-N and Hwang B-J 2016 Using hematite for photoelectrochemical water splitting: a review of current progress and challenges *Nanoscale Horiz.* **1** 243–67
- [20] Cheng L, Xiang Q, Liao Y and Zhang H 2018 CdS-based photocatalysts *Energy Environ. Sci.* **11** 1362–91
- [21] Ong W-J, Tan L-L N Y, Yong S-T H and Chai S-P 2016 Graphitic carbon nitride (g-C₃N₄)-based photocatalysts for artificial photosynthesis and environmental remediation: are we a step closer to achieving sustainability? *Chem. Rev.* **116** 7159–329
- [22] de Jongh P E, Vanmaekelbergh D and Kelly J J 2000 Photoelectrochemistry of electrodeposited Cu₂O *J. Electrochem. Soc.* **147** 486
- [23] Nemoto J, Gokan N, Ueno H and Kaneko M 2007 Photodecomposition of ammonia to dinitrogen and dihydrogen on platinumized TiO₂ nanoparticles in an aqueous solution *J. Photochem. Photobiol. A* **185** 295–300
- [24] Kim J, Monllor-Satoca D and Choi W 2012 Simultaneous production of hydrogen with the degradation of organic pollutants using TiO₂ photocatalyst modified with dual surface components *Energy Environ. Sci.* **5** 7647–56
- [25] Kondarides D I, Daskalaki V M, Patsoura A and Veyrakis X E 2008 Hydrogen production by photo-induced reforming of biomass components and derivatives at ambient conditions *Catal. Lett.* **122** 26–32
- [26] Fu X, Long J, Wang X, Leung D Y C, Ding Z, Wu L, Zhang Z, Li Z and Fu X 2008 Photocatalytic reforming of biomass: a systematic study of hydrogen evolution from glucose solution *Int. J. Hydrog. Energy* **33** 6484–91
- [27] Hashimoto K, Kawai T and Sakata T 1984 Photocatalytic reactions of hydrocarbons and fossil fuels with water. Hydrogen production and oxidation *J. Phys. Chem.* **88** 4083–8
- [28] Li Y, Lu G and Li S 2003 Photocatalytic production of hydrogen in single component and mixture systems of electron donors and monitoring adsorption of donors by *in situ* infrared spectroscopy *Chemosphere* **52** 843–50
- [29] Badawy M I, Ghaly M Y and Ali M E M 2011 Photocatalytic hydrogen production over nanostructured mesoporous titania from olive mill wastewater *Desalination* **267** 250–5
- [30] Liu C, Lei Z, Yang Y and Zhang Z 2013 Preliminary trial on degradation of waste activated sludge and simultaneous hydrogen production in a newly-developed solar photocatalytic reactor with AgX/TiO₂-coated glass tubes *Water Res.* **47** 4986–92
- [31] Ryu S Y, Balcerski W, Lee T K and Hoffmann M R 2007 Photocatalytic production of hydrogen from water with visible light using hybrid catalysts of CdS attached to microporous and mesoporous silicas *J. Phys. Chem. C* **111** 18195–203
- [32] Cebada S, Soto E, Mota N, Garcia Fierro J L and Navarro R M 2020 ScienceDirect Effect of photodeposition conditions on Ni-CdS photocatalysts and its role in the photoactivity for H₂ production from ethanolic solutions *Int. J. Hydrogen Energy* **45** 20536–48
- [33] Lv H, Huang Y, Koodali R T, Liu G, Zeng Y, Meng Q and Yuan M 2020 Synthesis of sulfur-doped 2D graphitic carbon nitride nanosheets for efficient photocatalytic degradation of phenol and hydrogen evolution *ACS Appl. Mater. Interfaces* **12** 12656–67
- [34] Jiménez-Rangel K, Samaniego-Benítez J E, Lartundo-Rojas L, Calderón H A and Mantilla A 2020 Ternary g-C₃N₄/NiOOH/Ag nanocomposite photocatalyst with efficient charges separation and high activity for H₂ production *Fuel* **280** 118672
- [35] Ma Y, Wang X, Jia Y, Chen X, Han H and Li C 2014 Titanium dioxide-based nanomaterials for photocatalytic fuel generations *Chem. Rev.* **114** 9987–10043
- [36] Morikawa T, Asahi R, Ohwaki T, Aoki K and Taga Y 2001 Band-gap narrowing of titanium dioxide by nitrogen doping *Jpn. J. Appl. Phys.* **40** L561–3
- [37] Devi L G and Kavitha R 2013 A review on non metal ion doped titania for the photocatalytic degradation of organic pollutants under UV/solar light: role of photogenerated charge carrier dynamics in enhancing the activity *Appl. Catal. B* **140–141** 559–87
- [38] Sakthivel S and Kisch H 2003 Daylight photocatalysis by carbon-modified titanium dioxide *Angew. Chem. Int. Ed.* **42** 4908–11
- [39] Umebayashi T, Yamaki T, Itoh H and Asai K 2002 Band gap narrowing of titanium dioxide by sulfur doping *Appl. Phys. Lett.* **81** 454–6
- [40] Etacheri V, Seery M K, Hinder S J and Pillai S C 2011 Oxygen rich titania: a dopant free, high temperature stable, and visible-light active anatase photocatalyst *Adv. Funct. Mater.* **21** 3744–52
- [41] Zhu J and Zäch M 2009 Nanostructured materials for photocatalytic hydrogen production *Curr. Opin. Colloid Interface Sci.* **14** 260–9
- [42] Li X, Xia T, Xu C, Murowchick J and Chen X 2014 Synthesis and photoactivity of nanostructured CdS–TiO₂ composite catalysts *Catal. Today* **225** 64–73
- [43] Yang J, Yan H, Wang X, Wen F, Wang Z, Fan D, Shi J and Li C 2012 Roles of cocatalysts in Pt–PdS/CdS with exceptionally high quantum efficiency for photocatalytic hydrogen production *J. Catal.* **290** 151–7
- [44] Tang Y, Hu X and Liu C 2014 Perfect inhibition of CdS photocorrosion by graphene sheltering engineering on TiO₂ nanotube array for highly stable photocatalytic activity *Phys. Chem. Chem. Phys.* **16** 25321–9
- [45] Wu A, Tian C, Jiao Y, Yan Q, Yang G and Fu H 2017 Sequential two-step hydrothermal growth of MoS₂/CdS core-shell heterojunctions for efficient visible light-driven photocatalytic H₂ evolution *Appl. Catal. B* **203** 955–63
- [46] Dong G, Zhang Y, Pan Q and Qiu J 2014 A fantastic graphitic carbon nitride (g-C₃N₄) material: electronic structure, photocatalytic and photoelectronic properties *J. Photochem. Photobiol. C* **20** 33–50
- [47] Cao S and Yu J 2014 g-C₃N₄-based photocatalysts for hydrogen generation *J. Phys. Chem. Lett.* **5** 2101–7

- [48] Ge L, Zuo F, Liu J, Ma Q, Wang C, Sun D, Bartels L and Feng P 2012 Synthesis and efficient visible light photocatalytic hydrogen evolution of Polymeric g-C₃N₄ coupled with CdS quantum dots *J. Phys. Chem. C* **116** 13708–14
- [49] Wang J, Huang J, Xie H and Qu A 2014 Synthesis of g-C₃N₄/TiO₂ with enhanced photocatalytic activity for H₂ evolution by a simple method *Int. J. Hydrog. Energy* **39** 6354–63
- [50] Marugán J, van Grieken R, Cassano A E and Alfano O M 2016 Chapter 15—Photocatalytic Reactor Design *Photocatalysis: Fundamentals and Perspectives* (London: The Royal Society of Chemistry) pp 367–87
- [51] Giménez S and Bisquert J 2016 *Photoelectrochemical Solar Fuel Production* (Berlin: Springer)
- [52] Lianos P 2017 Review of recent trends in photoelectrocatalytic conversion of solar energy to electricity and hydrogen *Appl. Catal. B* **210** 235–54
- [53] van de Krol R and Grätzel M 2012 *Photoelectrochemical Hydrogen Production* (Berlin: Springer)
- [54] Kaneko M, Gokan N, Katakura N, Takei Y and Hoshino M 2005 Artificial photochemical nitrogen cycle to produce nitrogen and hydrogen from ammonia by platinized TiO₂ and its application to a photofuel cell *Chem. Commun.* 1625–7
- [55] Wang G, Ling Y, Lu X, Wang H, Qian F, Tong Y and Li Y 2012 Solar driven hydrogen releasing from urea and human urine *Energy Environ. Sci.* **5** 8215–9
- [56] Pop L C, Tantis I and Lianos P 2015 Photoelectrocatalytic hydrogen production using nitrogen containing water soluble wastes *Int. J. Hydrog. Energy* **40** 8304–10
- [57] Wu Z, Zhao G, Zhang Y, Liu J, Zhang Y N and Shi H 2015 A solar-driven photocatalytic fuel cell with dual photoelectrode for simultaneous wastewater treatment and hydrogen production *J. Mater. Chem. A* **3** 3416–24
- [58] Liu X, Wang F and Wang Q 2012 Nanostructure-based WO₃ photoanodes for photoelectrochemical water splitting *Phys. Chem. Chem. Phys.* **14** 7894–911
- [59] Li Z, Luo W, Zhang M, Feng J and Zou Z 2013 Photoelectrochemical cells for solar hydrogen production: current state of promising photoelectrodes, methods to improve their properties, and outlook *Energy Environ. Sci.* **6** 347–70
- [60] Gan J, Lu X and Tong Y 2014 Towards highly efficient photoanodes: boosting sunlight-driven semiconductor nanomaterials for water oxidation *Nanoscale* **6** 7142–64
- [61] Vesborg P C K, Seger B and Chorkendorff I 2015 Recent development in hydrogen evolution reaction catalysts and their practical implementation *J. Phys. Chem. Lett.* **6** 951–7
- [62] Wang G, Ling Y, Lu X, Zhai T, Qian F, Tong Y and Li Y 2013 A mechanistic study into the catalytic effect of Ni(OH)₂ on hematite for photoelectrochemical water oxidation *Nanoscale* **5** 4129–33
- [63] Paramasivam I, Jha H, Liu N and Schmuki P 2012 A review of photocatalysis using self-organized TiO₂ nanotubes and other ordered oxide nanostructures *Small* **8** 3073–103
- [64] Sun Y, Murphy C J, Reyes-Gil K R, Reyes-Garcia E A, Thornton J M, Morris N A and Raftery D 2009 Photoelectrochemical and structural characterization of carbon-doped WO₃ films prepared via spray pyrolysis *Int. J. Hydrog. Energy* **34** 8476–84
- [65] Cole B, Marsen B, Miller E, Yan Y, To B, Jones K and Al-Jassim M 2008 Evaluation of nitrogen doping of tungsten oxide for photoelectrochemical water splitting *J. Phys. Chem. C* **112** 5213–20
- [66] Su J, Guo L, Bao N and Grimes C A 2011 Nanostructured WO₃/BiVO₄ heterojunction films for efficient photoelectrochemical water splitting *Nano Lett.* **11** 1928–33
- [67] Walsh A, Yan Y, Huda M N, Al-Jassim M M and Wei S H 2009 Band edge electronic structure of BiVO₄: elucidating the role of the Bi s and V d orbitals *Chem. Mater.* **21** 547–51
- [68] Luo W, Yang Z, Li Z, Zhang J, Liu J, Zhao Z, Wang Z, Yan S, Yu T and Zou Z 2011 Solar hydrogen generation from seawater with a modified BiVO₄ photoanode *Energy Environ. Sci.* **4** 4046–51
- [69] Li M, Zhao L and Guo L 2010 Preparation and photoelectrochemical study of BiVO₄ thin films deposited by ultrasonic spray pyrolysis *Int. J. Hydrog. Energy* **35** 7127–33
- [70] Abdi F F and van de Krol R 2012 Nature and light dependence of bulk recombination in Co-Pi-catalyzed BiVO₄ photoanodes *J. Phys. Chem. C* **116** 9398–404
- [71] Chatchai P, Murakami Y, Kishioka S, Nosaka A Y and Nosaka Y 2009 Efficient photocatalytic activity of water oxidation over WO₃/BiVO₄ composite under visible light irradiation *Electrochim. Acta* **54** 1147–52
- [72] Chatchai P, Murakami Y, Kishioka S-Y, Nosaka A Y and Nosaka Y 2008 FTO/SnO₂/BiVO₄ composite photoelectrode for water oxidation under visible light irradiation *Electrochem. Solid-State Lett.* **11** H160
- [73] Shinar R and Kennedy J H 1982 Photoactivity of doped α -Fe₂O₃ electrodes *Sol. Energy Mater.* **6** 323–35
- [74] Kleiman-Shwarsstein A, Hu Y-S, Forman A J, Stucky G D and McFarland E W 2008 Electrodeposition of α -Fe₂O₃ doped with Mo or Cr as photoanodes for photocatalytic water splitting *J. Phys. Chem. C* **112** 15900–7
- [75] Sanchez C, Sieber K D and Somorjai G A 1988 The photoelectrochemistry of niobium doped α -Fe₂O₃ *J. Electroanal. Chem. Interfacial Electrochem.* **252** 269–90
- [76] Zhong D K, Cornuz M, Sivula K, Grätzel M and Gamelin D R 2011 Photo-assisted electrodeposition of cobalt-phosphate (Co-Pi) catalyst on hematite photoanodes for solar water oxidation *Energy Environ. Sci.* **4** 1759–64
- [77] Le Formal F, Tétreault N, Cornuz M, Moehl T, Grätzel M and Sivula K 2011 Passivating surface states on water splitting hematite photoanodes with alumina overlayers *Chem. Sci.* **2** 737–43
- [78] Huang Q, Ye Z and Xiao X 2015 Recent progress in photocathodes for hydrogen evolution *J. Mater. Chem. A* **3** 15824–37
- [79] Paracchino A, Laporte V, Sivula K, Grätzel M and Thimsen E 2011 Highly active oxide photocathode for photoelectrochemical water reduction *Nat. Mater.* **10** 456–61
- [80] Li C, Hisatomi T, Watanabe O, Nakabayashi M, Shibata N, Domen K and Delaunay J J 2016 Simultaneous enhancement of photovoltage and charge transfer in Cu₂O-based photocathode using buffer and protective layers *Appl. Phys. Lett.* **109** 033902
- [81] Chen Y, Feng X, Liu M, Su J and Shen S 2016 Towards efficient solar-to-hydrogen conversion: fundamentals and recent progress in copper-based chalcogenide photocathodes *Nanophotonics* **5** 468–91
- [82] Yang C, Iran P D, Boix P P, Bassi P S, Yantara N, Wong L H and Barber J 2014 Engineering a Cu₂O/NiO/Cu₂MoS₄ hybrid photocathode for H₂ generation in water *Nanoscale* **6** 6506–10
- [83] Chen Y, Feng X, Liu M, Su J and Shen S 2016 Towards efficient solar-to-hydrogen conversion: fundamentals and recent progress in copper-based chalcogenide photocathodes *Nanophotonics* **5** 524–47
- [84] Yokoyama D, Minegishi T, Maeda K, Katayama M, Kubota J, Yamada A, Konagai M and Domen K 2010 Photoelectrochemical water splitting using a Cu(In,Ga)Se₂ thin film *Electrochem. Commun.* **12** 851–3
- [85] Wang J, Yu N, Zhang Y, Zhu Y, Fu L, Zhang P, Gao L and Wu Y 2016 Synthesis and performance of Cu₂ZnSnS₄ semiconductor as photocathode for solar water splitting *J. Alloys Compd.* **688** 923–32
- [86] Sabatier P 1911 Hydrogénations et déshydrogénations par catalyse *Berichte Der Dtsch. Chem. Gesellschaft* **44** 1984–2001

- [87] Greeley J, Jaramillo T F, Bonde J, Chorkendorff I and Nørskov J K 2006 Computational high-throughput screening of electrocatalytic materials for hydrogen evolution *Nat. Mater.* **5** 909–13
- [88] Raj I A and Vasu K I 1990 Transition metal-based hydrogen electrodes in alkaline solution—electrocatalysis on nickel based binary alloy coatings *J. Appl. Electrochem.* **20** 32–38
- [89] Hinnemann B, Moses P G, Bonde J, Jørgensen K P, Nielsen J H, Horch S, Chorkendorff I and Nørskov J K 2005 Biomimetic hydrogen evolution: MoS₂ nanoparticles as catalyst for hydrogen evolution *J. Am. Chem. Soc.* **127** 5308–9
- [90] Voiry D et al 2013 Enhanced catalytic activity in strained chemically exfoliated WS₂ nanosheets for hydrogen evolution *Nat. Mater.* **12** 850–5
- [91] Tsai C, Chan K, Abild-Pedersen F and Nørskov J K 2014 Active edge sites in MoSe₂ and WSe₂ catalysts for the hydrogen evolution reaction: a density functional study *Phys. Chem. Chem. Phys.* **16** 13156–64
- [92] Trasatti S 1972 Work function, electronegativity, and electrochemical behaviour of metals: III. Electrolytic hydrogen evolution in acid solutions *J. Electroanal. Chem. Interfacial Electrochem.* **39** 163–84
- [93] Popczun E J, McKone J R, Read C G, Biacchi A J, Wiltrout A M, Lewis N S and Schaak R E 2013 nanostructured nickel phosphide as an electrocatalyst for the hydrogen evolution reaction *J. Am. Chem. Soc.* **135** 9267–70
- [94] Zheng Y, Jiao Y, Li L H, Xing T, Chen Y, Jaroniec M and Qiao S Z 2014 Toward design of synergistically active carbon-based catalysts for electrocatalytic hydrogen evolution *ACS Nano* **8** 5290–6
- [95] Shalom M, Gimenez S, Schipper F, Herranz-Cardona I, Bisquert J and Antonietti M 2014 Controlled carbon nitride growth on surfaces for hydrogen evolution electrodes *Angew. Chem. Int. Ed.* **53** 3654–8
- [96] Henze M, van Loosdrecht M C, Ekama G A and Brdjanovic D 2008 *Biological Wastewater Treatment: Principles, Modelling and Design* (London: IWA Publishing)
- [97] European Environment Agency 2018 Industrial waste water treatment—pressures on Europe’s environment *EEA Report No. 23/2018* (Copenhagen: EEA)
- [98] Cervantes F J (ed) 2009 *Environmental Technologies to Treat Nitrogen Pollution* (London: IWA Publishing)
- [99] Camargo J A and Alonso Á 2006 Ecological and toxicological effects of inorganic nitrogen pollution in aquatic ecosystems: a global assessment *Environ. Int.* **32** 831–49
- [100] Zhu X, Castleberry S R, Nanny M A and Butler E C 2005 Effects of pH and catalyst concentration on photocatalytic oxidation of aqueous ammonia and nitrite in titanium dioxide suspensions *Environ. Sci. Technol.* **39** 3784–91
- [101] Wang H, Su Y, Zhao H, Yu H, Chen S, Zhang Y and Quan X 2014 Photocatalytic oxidation of aqueous ammonia using atomic single layer graphitic-C₃N₄ *Environ. Sci. Technol.* **48** 11984–90
- [102] Altomare M and Selli E 2013 Effects of metal nanoparticles deposition on the photocatalytic oxidation of ammonia in TiO₂ aqueous suspensions *Catal. Today* **209** 127–33
- [103] Yuzawa H, Mori T, Itoh H and Yoshida H 2012 Reaction mechanism of ammonia decomposition to nitrogen and hydrogen over metal loaded titanium oxide photocatalyst *J. Phys. Chem. C* **116** 4126–36
- [104] Shiraishi Y, Toi S, Ichikawa S and Hirai T 2020 Photocatalytic NH₃ splitting on TiO₂ particles decorated with Pt-Au bimetallic alloy nanoparticles *ACS Appl. Nano Mater.* **3** 1612–20
- [105] Wang H, Zhang X, Su Y, Yu H, Chen S, Quan X and Yang F 2014 Photoelectrocatalytic oxidation of aqueous ammonia using TiO₂ nanotube arrays *Appl. Surf. Sci.* **311** 851–7
- [106] Xu D, Fu Z, Wang D, Lin Y, Sun Y, Meng D and Feng Xie T 2015 A Ni(OH)₂-modified Ti-doped α-Fe₂O₃ photoanode for improved photoelectrochemical oxidation of urea: the role of Ni(OH)₂ as a cocatalyst *Phys. Chem. Chem. Phys.* **17** 23924–30
- [107] Gupta M, Ho D, Santoro D, Torfs E, Doucet J, Vanrolleghem P A and Nakhla G 2018 Experimental assessment and validation of quantification methods for cellulose content in municipal wastewater and sludge *Environ. Sci. Pollut. Res.* **25** 16743–53
- [108] Kawai T and Sakata T 1980 Conversion of carbohydrate into hydrogen fuel by a photocatalytic process *Nature* **286** 474–6
- [109] Speltini A, Sturini M, Dondi D, Annovazzi E, Maraschi F, Caratto V, Profumo A and Buttafava A 2014 Sunlight-promoted photocatalytic hydrogen gas evolution from water-suspended cellulose: a systematic study *Photochem. Photobiol. Sci.* **13** 1410–9
- [110] Caravaca A, Jones W, Hardacre C and Bowker M 2016 H₂ production by the photocatalytic reforming of cellulose and raw biomass using Ni, Pd, Pt and Au on titania *Proc. R. Soc. A: Mathematical, Physical and Engineering Sciences* **472** 20160054
- [111] Chong R, Li J, Ma Y, Zhang B, Han H and Li C 2014 Selective conversion of aqueous glucose to value-added sugar aldose on TiO₂-based photocatalysts *J. Catal.* **314** 101–8
- [112] Imizcoz M and Puga A V 2019 Assessment of photocatalytic hydrogen production from biomass or wastewaters depending on the metal co-catalyst and its deposition method on TiO₂ *Catalysts* **9** 584
- [113] Bahadori E, Ramis G, Zanardo D, Menegazzo F, Signoretti M, Gazzoli D, Pietrogiacomini D, Michele A D and Rossetti I 2020 Photoreforming of glucose over CuO/TiO₂ *Catalysts* **10** 477
- [114] Esposito D V, Forest R V, Chang Y, Gaillard N, McCandless B E, Hou S, Lee K H, Birkmire R W and Chen J G 2012 Photoelectrochemical reforming of glucose for hydrogen production using a WO₃-based tandem cell device *Energy Environ. Sci.* **5** 9091–9
- [115] Villegas L G C, Mashhadi N, Chen M, Mukherjee D, Taylor K E and Biswas N 2016 A short review of techniques for phenol removal from wastewater *Curr. Pollut. Rep.* **2** 157–67
- [116] Duan W, Meng F, Cui H, Lin Y, Wang G and Wu J 2018 Ecotoxicity of phenol and cresols to aquatic organisms: a review *Ecotoxicol. Environ. Saf.* **157** 441–56
- [117] Ahmed S, Rasul M G, Martens W N, Brown R and Hashib M A 2010 Heterogeneous photocatalytic degradation of phenols in wastewater: a review on current status and developments *Desalination* **261** 3–18
- [118] Park H, Bak A, Ahn Y Y, Choi J and Hoffmann M R 2012 Photoelectrochemical performance of multi-layered BiO_x-TiO₂/Ti electrodes for degradation of phenol and production of molecular hydrogen in water *J. Hazard. Mater.* **211–212** 47–54
- [119] Languer M P, Scheffer F R, Feil A F, Baptista D L, Migowski P, Machado G J, De Moraes D P, Dupont J, Teixeira S R and Weibel D E 2013 Photo-induced reforming of alcohols with improved hydrogen apparent quantum yield on TiO₂ nanotubes loaded with ultra-small Pt nanoparticles *Int. J. Hydrog. Energy* **38** 14440–50
- [120] Li F, Zhao W and Leung D Y C 2019 Enhanced photoelectrocatalytic hydrogen production via Bi/BiVO₄ photoanode under visible light irradiation *Appl. Catal. B* **258** 117954
- [121] Daud N M, Sheikh Abdullah S R, Abu Hasan H and Yaakob Z 2015 Production of biodiesel and its wastewater treatment technologies: a review *Process Saf. Environ. Prot.* **94** 487–508
- [122] Kawai T and Sakata T 1980 Photocatalytic hydrogen production from liquid methanol and water *J. Chem. Soc., Chem. Commun.* 694–5

- [123] Chiarello G L, Aguirre M H and Selli E 2010 Hydrogen production by photocatalytic steam reforming of methanol on noble metal-modified TiO₂ *J. Catal.* **273** 182–90
- [124] Naldoni A, D'Arienzo M, Altomare M, Marelli M, Scotti R, Morazzoni F, Selli E and Dal Santo V 2013 Pt and Au/TiO₂ photocatalysts for methanol reforming: role of metal nanoparticles in tuning charge trapping properties and photoefficiency *Appl. Catal. B* **130–131** 239–48
- [125] Chen T, Feng Z, Wu G, Shi J, Ma G, Ying P and Li C 2007 Mechanistic studies of photocatalytic reaction of methanol for hydrogen production on Pt/TiO₂ by *in situ* Fourier transform IR and time-resolved IR spectroscopy *J. Phys. Chem. C* **111** 8005–14
- [126] Ismael M 2019 Highly effective ruthenium-doped TiO₂ nanoparticles photocatalyst for visible-light-driven photocatalytic hydrogen production *New J. Chem.* **43** 9596–605
- [127] Chen S, Li X, Zhou W, Zhang S and Fang Y 2019 Carbon-coated Cu-TiO₂ nanocomposite with enhanced photostability and photocatalytic activity *Appl. Surf. Sci.* **466** 254–61
- [128] Liu Y, Ye Z, Li D, Wang M, Zhang Y and Huang W 2019 Tuning CuO_x-TiO₂ interaction and photocatalytic hydrogen production of CuO_x/TiO₂ photocatalysts via TiO₂ morphology engineering *Applied Surface Science* **473** 500–10
- [129] Hojamberdiev M, Khan M M, Kadirova Z, Kawashima K, Yubuta K, Teshima K, Riedel R and Hasegawa M 2019 Synergistic effect of g-C₃N₄, Ni(OH)₂ and halloysite in nanocomposite photocatalyst on efficient photocatalytic hydrogen generation *Renew. Energy* **138** 434–44
- [130] Sakata T and Kawai T 1981 Heterogeneous photocatalytic production of hydrogen and methane from ethanol and water *Chem. Phys. Lett.* **80** 341–4
- [131] Yang Y Z, Chang C H and Idriss H 2006 Photo-catalytic production of hydrogen from ethanol over M/TiO₂ catalysts (M = Pd, Pt or Rh) *Appl. Catal. B* **67** 217–22
- [132] Sola A C, Ramírez de la Piscina P and Homs N 2020 Behaviour of Pt/TiO₂ catalysts with different morphological and structural characteristics in the photocatalytic conversion of ethanol aqueous solutions *Catal. Today* **341** 13–20
- [133] Puga A V, Forneli A, García H and Corma A 2014 Production of H₂ by ethanol photoreforming on Au/TiO₂ *Adv. Funct. Mater.* **24** 241–8
- [134] Deas R, Pearce S, Goss K, Wang Q, Chen W T and Waterhouse G I N 2020 Hierarchical Au/TiO₂ nanoflower photocatalysts with outstanding performance for alcohol photoreforming under UV irradiation *Appl. Catal. A* **602** 39–41
- [135] Pajares A, Wang Y, Kronenberg M J, Ramírez de la Piscina P and Homs N 2020 Photocatalytic H₂ production from ethanol aqueous solution using TiO₂ with tungsten carbide nanoparticles as co-catalyst *Int. J. Hydrogen Energy* **45** 20558–67
- [136] Zhang X, Luo L, Yun R, Pu M, Zhang B and Xiang X 2019 Increasing the activity and selectivity of TiO₂-supported Au catalysts for renewable hydrogen generation from ethanol photoreforming by engineering Ti³⁺ defects *ACS Sustain. Chem. Eng.* **7** 13856–64
- [137] Antoniadou M, Bouras P, Strataki N and Lianos P 2008 Hydrogen and electricity generation by photoelectrochemical decomposition of ethanol over nanocrystalline titania *Int. J. Hydrog. Energy* **33** 5045–51
- [138] Marios Adamopoulos P, Papagiannis I, Raptis D and Lianos P 2019 Photoelectrocatalytic hydrogen production using a TiO₂/WO₃ bilayer photocatalyst in the presence of ethanol as a fuel *Catalysts* **9** 1–12
- [139] Fu X, Wang X, Leung D Y C, Gu Q, Chen S and Huang H 2011 Photocatalytic reforming of C₃-polyols for H₂ production. Part (I). Role of their OH groups *Appl. Catal. B* **106** 681–8
- [140] Bowker M, Davies P R and Al-Mazroai L S 2009 Photocatalytic reforming of glycerol over gold and palladium as an alternative fuel source *Catal. Lett.* **128** 253–5
- [141] Montini T, Gombac V, Sordelli L, Delgado J J, Chen X, Adami G and Fornasiero P 2011 Nanostructured Cu/TiO₂ photocatalysts for H₂ production from ethanol and glycerol aqueous solutions *ChemCatChem* **3** 574–7
- [142] Chen W T, Dong Y, Yadav P, Aughterson R D, Sun-Waterhouse D and Waterhouse G I N 2020 Effect of alcohol sacrificial agent on the performance of Cu/TiO₂ photocatalysts for UV-driven hydrogen production *Appl. Catal. A* **602** 117703
- [143] Daskalaki V M and Kondarides D I 2009 Efficient production of hydrogen by photo-induced reforming of glycerol at ambient conditions *Catal. Today* **144** 75–80
- [144] Naffati N, Sampaio M J, Da Silva E S, Nsib M F, Arfaoui Y, Houas A, Faria J L and Silva C G 2020 Carbon-nanotube/TiO₂ materials synthesized by a one-pot oxidation/hydrothermal route for the photocatalytic production of hydrogen from biomass derivatives *Mater. Sci. Semicond. Process* **115** 105098
- [145] Mohapatra S K, Raja K S, Mahajan V K and Misra M 2008 Efficient photoelectrolysis of water using TiO₂ nanotube arrays by minimizing recombination losses with organic additives *J. Phys. Chem. C* **112** 11007–12
- [146] Antoniadou M and Lianos P 2009 Near ultraviolet and visible light photoelectrochemical degradation of organic substances producing electricity and hydrogen *J. Photochem. Photobiol. A* **204** 69–74
- [147] Narkis N, Henefeld-Fourrier S and Rebhun M 1980 Volatile organic acids in raw wastewater and in physico-chemical treatment *Water Res.* **14** 1215–23
- [148] Garrido J M, Méndez R and Lema J M 2000 Treatment of wastewaters from a formaldehyde-urea adhesives factory *Water Sci. Technol.* **42** 293–300
- [149] Patsoura A, Kondarides D I and Verykios X E 2007 Photocatalytic degradation of organic pollutants with simultaneous production of hydrogen *Catal. Today* **124** 94–102
- [150] Imizcoz M and Puga A V 2019 Optimising hydrogen production: via solar acetic acid photoreforming on Cu/TiO₂ *Catal. Sci. Technol.* **9** 1098–102
- [151] Speltini A, Sturini M, Maraschi F, Dondi D, Fisogni G, Annovazzi E, Profumo A and Buttafava A 2015 Evaluation of UV-A and solar light photocatalytic hydrogen gas evolution from olive mill wastewater *Int. J. Hydrog. Energy* **40** 4303–10
- [152] Ntaikou I, Kourmentza C, Koutrouli E C, Stamatelatu K, Zampraka A, Kornaros M and Lyberatos G 2009 Exploitation of olive oil mill wastewater for combined biohydrogen and biopolymers production *Bioresour. Technol.* **100** 3724–30